WORLD RESOURCES INSTITUTE

TECHNICAL NOTE

City-scale, city-relevant climate hazard indicators under 1.5°C, 2.0°C, and 3.0°C of global warming

Theodore Wong and Eric Mackres

CONTENTS

Technical notes document the research or analytical methodology underpinning a publication, interactive application, or tool.

Suggested Citation: Wong, T. and E. Mackres. 2024. "City-scale, city-relevant climate hazard indicators under 1.5°C, 2.0°C, and 3.0°C of global warming." Technical Note. Washington, DC: World Resources Institute. Available online at: doi.org/10.46830/writn.23.00154.

ABSTRACT

We present a data set reporting estimates of average values of 14 temperature-, humidity- and precipitation-based climate hazards for the world's most populous 996 cities under three global warming scenarios: 1.5°C, 2.0°C, and 3.0°C above a preindustrial (1880–1900) baseline. We also report probabilities that the hazard magnitudes exceed certain extreme values. The hazards focus on themes of operational and planning relevance to city government decision-makers in public health, infrastructure, and economic productivity. Hazard magnitude probabilities were estimated from probability models parameterized from three downscaled global climate models (from NEX-GDDP-CMIP6) determined to be most appropriate for each location based on comparison with historical reanalysis data. Across all 996 cities studied, heat waves become, on average, longer and more frequent as the world warms. Number of days with optimal temperature for the malaria vector *Anopheles gambiae* decreases modestly, but days with optimal temperature for the arbovirus vectors *Aedes aegypti* and *Aedes albopictus* become more frequent. Precipitation-based hazards change little when averaged across all 996 cities, but differences arise when cities are disaggregated by region or income level. We provide the data publicly to aid decision-makers in climate action planning and to illustrate the dire consequences for cities if global warming is allowed to exceed the 1.5°C Paris Agreement target.

OVERVIEW

In the global climate policy discourse, outcome targets are frequently expressed in terms of global mean surface temperature (GMST). The 2015 Paris Agreement, for example, establishes a target to limit global warming to 1.5°C above the preindustrial average (UNFCCC 2016), and a great deal of research has focused on identifying the policies and actions that are compatible with that target (e.g., Millar et al. 2017; Tilmes et al. 2020; Meinshausen et al. 2022; Riahi et al. 2022). As an indicator, GMST is convenient and useful—it encapsulates in a single number the degree to which the climate has changed from a preindustrial baseline. It does not, however, directly provide decision-makers

or the public with specific information about the climate futures they or their constituents will face or the local consequences to ecosystems, people, or economies. Moreover, analyses of the consequences of increasing GMST for ecosystems and societies have tended to be global or regional in scale (Arnell et al. 2018; IPCC 2018) and have focused on regional systems such as agriculture or water (Schleussner et al. 2016; Ren et al. 2018).

We are publishing a data set[1] that estimates climate hazard magnitudes that cities will face as GMST increases. For three warming levels—+1.5°C, +2.0°C, and +3.0°C—we estimated the average values of 14 city-relevant climate hazards for the world's most populous 996 cities. For each city, we also estimated the probabilities that hazard magnitude values exceed particular extreme thresholds. The hazards were chosen to address climate adaptation decision-making in public health, infrastructure maintenance, and economic productivity. Local decision-makers in the included cities can use the estimates to guide planning and policy for climate adaptation and mitigation. The estimates also predict clear differences between the +1.5°C and +3.0°C scenarios. Differences in direction and degree of change exist when cities are disaggregated by region and income level; yet in general, urban dwellers in a +3.0°C world will see greater extremes of high temperature, as well as a modest increase in drought, compared to the +1.5°C scenario.

METHODS

City selection

Our analysis encompasses the 996 cities globally (Figure 1) whose 2015 populations were greater than 500,000 according to the Global Human Settlement Layer (GHSL) Urban Centre Database, version 1.2 (Florczyk et al. 2019). The cities include roughly 2 billion people, or 56 percent of the roughly 3.5 billion urban dwellers represented in the cities of the database. We chose this data set because it is currently the only global data set that spatially delineates urban areas and associates them with place names. Cities are defined in the Urban Centre Database based on resident population and built-up land share, and they are metropolitan areas rather than cities as defined by administrative boundaries. Our indicator calculation method uses point locations, so we used the centroid of each GHSL urban-center polygon to estimate the climate hazard probabilities. We acknowledge that our approach does not support within-city analyses, but researchers focusing on one city or region might be able to obtain high-resolution climate simulations—for example, from regional models—and apply our methods to obtain high-resolution results.

Figure 1 | **Cities included in this study**

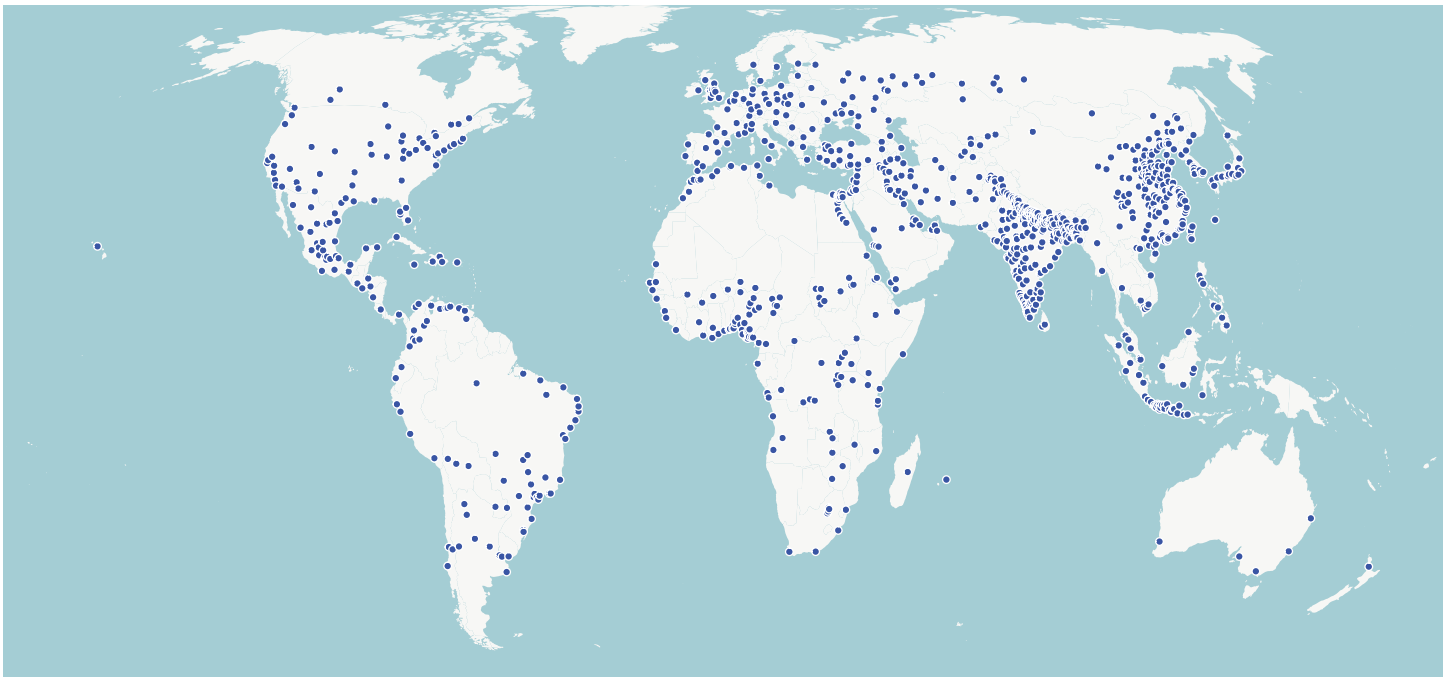

Note: For the study, 996 cities were chosen for having populations larger than 500,000 in 2015, according to the Global Human Settlement Layer Urban Centre Database.
Source: Florczyk et al. 2019.

Models

All estimates of future hazards are calculated from nine global climate models included in the NEX-GDDP-CMIP6 collection of downscaled model outputs (Thrasher et al. 2022). NEX-GDDP-CMIP6 is frequently used in local-scale climate impact studies (e.g., Zhang et al. 2023, Paul and Maity 2023, Rao et al. 2024). All NEX-GDDP-CMIP6 models have a horizontal spatial resolution of 0.25 degrees. The corresponding ground distance varies by latitude but is approximately 25 kilometers for many of our cities. These model outputs include daily minimum, maximum, and mean air temperature at two meters above Earth's surface; daily cumulative precipitation; average daily relative humidity; and average daily wind speed.

As processed for storage in Google Earth Engine (Gorelick et al. 2017), the model outputs are available as daily values for the period 1950–2100 for the historical scenario and for two greenhouse gas emissions scenarios. For the years 2015–2100, the greenhouse gas emissions scenario can be specified as either of two Shared Socioeconomic Pathway (SSP) scenarios: SSP2-4.5 or SSP5-8.5 (see Riahi et al. [2017] for discussion of SSP scenarios).

Kuma et al. (2023) found that models derived from the same original code—that is, members of the same model families—can produce results that are more similar to each other than models of different families. Failure to account for similarities within model families can lead to underestimating uncertainty in predictions. NEX-GDDP-CMIP6 includes 35 models, which represent nine model families. To avoid oversampling any particular model family, and because the scope of this project required us to limit the models to a manageable number, we used only one randomly chosen model from each of the nine model families. Table 1 lists the selected models, their families, and the research institutions that created and maintain them.

Table 1 | **Climate models included in NEX-GDDP-CMIP6, with model families**

MODEL	MODEL FAMILY	INSTITUTION
CanESM5	CanAM	Canadian Centre for Climate Modelling and Analysis
EC-Earth3-Veg-LR	ECMWF	EC-Earth Consortium (Agencia Estatal de Meteorología, Spain; Barcelona Supercomputing Center, Spain; Consiglio Nazionale delle Ricerche–Instituto di Scienze dell'Atmosfera e del Clima, Italy; Danish Meteorological Institute, Denmark; Ente per le Nuove Technologie l'Energia e l'Ambiente, Italy; Finnish Meteorological Institute, Finland; Geomar, Germany; Irish Centre for High-End Computing, Ireland; International Centre for Theoretical Physics, Italy; Instituto Dom Luiz, Portugal; Institute for Marine and Atmospheric research Utrecht, Netherlands; Instituto Português do Mar e da Atmosfera, Portugal; Karlsruhe Institute of Technology, Germany; Royal Netherlands Meteorological Institute, Netherlands; Lund University, Sweden; Met Eireann, Ireland; Netherlands eScience Center, Netherlands; Norwegian University of Science and Technology, Norway; Oxford University, United Kingdom; SURFsara, Netherlands; Swedish Meteorological and Hydrological Institute, Sweden; Stockholm University, Sweden; Unite ASTR, Belgium; University College Dublin, Ireland; University of Bergen, Norway; University of Copenhagen, Denmark; University of Helsinki, Finland; University of Santiago de Compostela, Spain; Uppsala University, Sweden; Utrecht University, Netherlands; Vrije Universiteit Amsterdam, Netherlands; Wageningen University, Netherlands)
FGOALS-g3	CCM	Chinese Academy of Sciences
GFDL-ESM4	GFDL	National Oceanic and Atmospheric Administration (United States), Geophysical Fluid Dynamics Laboratory
INM-CM5-0	INM	Institute for Numerical Mathematics, Russian Academy of Science
IPSL-CM6A-LR	IPSL	Institut Pierre Simon Laplace
MIROC-ES2L	MIROC	Japan Agency for Marine-Earth Science and Technology
MRI-ESM2-0	UCLA GCM	Meteorological Research Institute (Japan)
UKESM1-0-LL	HadAM	Met Office Hadley Centre; Natural Environment Research Council (United Kingdom); National Institute of Meteorological Sciences/Korea Meteorological Administration

Notes: We acknowledge the World Climate Research Programme, which, through its Working Group on Coupled Modelling, coordinated and promoted the Coupled Model Intercomparison Project Phase 6 (CMIP6). We thank the climate modeling groups for producing and making available their model output, the Earth System Grid Federation (ESGF) for archiving the data and providing access, and the multiple funding agencies that support CMIP6 and ESGF. Model families are from Kuma et al. (2023).

Warming scenario years

Assessing climate futures at various GMST values requires projections for future meteorological conditions that are associated with those GMSTs. One could identify two general approaches to obtaining or identifying the relevant meteorological projections: generating climate model data specifically for target GMSTs or examining climate models that at some point exceed target GMSTs and then identifying time intervals whose time-averaged GMSTs correspond to the GMSTs of interest.

The first approach, which we did not take, finds or derives climate model runs that stabilize at the target GMST by a specified future year. The difficulty in this approach is that the major model intercomparison projects do not include model runs that correspond closely to all GMSTs of interest. Some studies (e.g., Mitchell et al. 2017; Sieck et al. 2021) address this issue by using weighted averages of the models that stabilize closest to the target GMSTs. Others (e.g., Sanderson 2017; Nangombe 2018) create simplified emulations of published global climate models and run the emulations with greenhouse gas emissions pathways that produce the desired equilibrium GMSTs. Both methods generate model outputs at the coarse spatial resolutions of global climate models, so using them for our city-focused study would require computationally expensive downscaling.

We took the second approach. Following Schleussner et al. (2016), Dosio et al. (2018), Jacob et al. (2018), and Li et al. (2022), we examined model runs that span our GMSTs of interest and identified within each of them multiyear periods with the average GMST values of interest. This approach allowed us to use the NEX-GDDP-CMIP6 models, which come with two advantages: they are downscaled to a city-relevant spatial scale, and we were able to access several independent models for each variable-location combination and select the models for each location that seem to minimize the unavoidable regional biases that all global climate models have. Note that it will often be the case that a single city's heat-based hazard indicators are estimated using different models from those used to estimate precipitation-based hazard indicators. This should create no difficulties as long as different hazard indicators are examined separately from each other. Specifically, indicators for different hazards should not be combined into compound indicators. For example, the probabilities of exceeding extreme-magnitude thresholds for two hazards should not be combined into a joint probability.

Specifically, for each of the NEX-GDDP-CMIP6 models we used, we calculated the model's recent historical reference period level as the average GMST over every day of the 20-year period 1995–2014. Dosio et al. (2018) estimate that the GMST in these 20 years, centered on 2005, is 0.81°C above a preindustrial baseline, so GMST values of +1.5°C, +2.0°C, and +3.0°C above the same preindustrial baseline correspond to these values minus the 2005 value, or +0.69°C, +1.19°C, and +2.19°C above the recent historical reference period level.

GMST was calculated in Google Earth Engine using the function *ee.Reducer.mean()* and applied to the average two-meter-height air temperature over the entire globe. For each year during the 2015–2091 period, we identified the first year at which the average exceeded +0.69°C, +1.19°C, and +2.19°C relative to the 20-year average GMST for 1995–2014. The time interval for which we estimate annual average climate hazard indicators was the 10-year interval centered on this year. (In the rest of this paper we refer to the warming scenarios by the GMSTs relative to the preindustrial baseline—that is, +1.5°C, +2.0°C, and +3.0°C—rather than by the GMSTs relative to 1995–2014.) For every model, the SSP2-4.5 emissions scenario allowed us to find 10-year intervals with little or no overlap between the +1.5°C and +2.0°C scenarios and between the +2.0°C and +3.0°C scenarios. For our purposes, only the degree to which Earth has warmed—and not the emissions pathway that caused the warming—is relevant.

Figure 3 represents the GMST trajectories for each of the model scenarios used, and Table 3 lists the center-point years of the time intervals corresponding to their GMST warming levels. For four of the models (MRI-ESM2-0, FGOALS-g3, IPSL-CM6A-LR, and CanESM5), there is some overlap between the +1.5°C and +2.0°C scenario intervals. In these cases it is difficult to distinguish between these warming levels.

Figure 2 | **GMST trajectories as modeled by the nine NEX-GDDP-CMIP6 models used in this study**

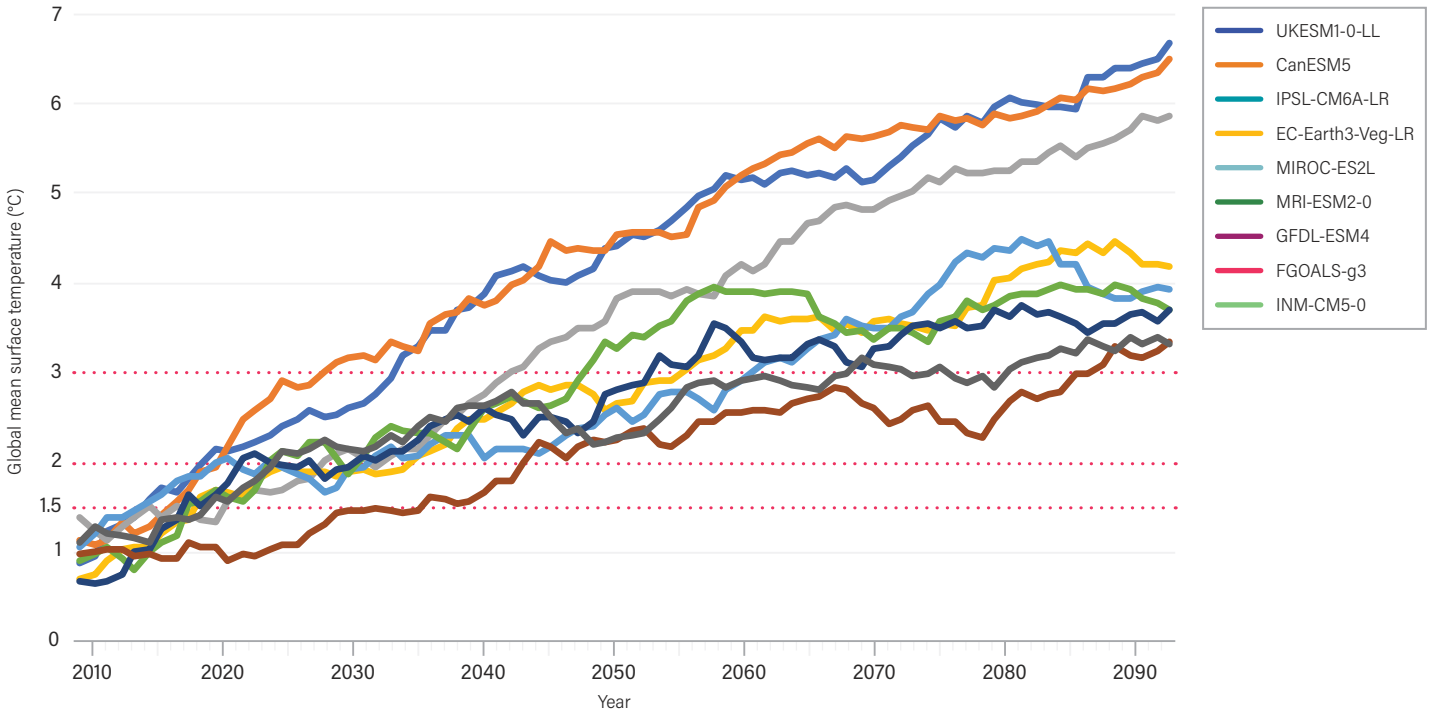

Notes: Temperatures from each model are given as changes relative to the 1880–1900 preindustrial baseline. Each model's +1.5°C, +2.0°C, and +3.0°C scenario years are the 10-year windows roughly centered on the year when the model first exceeds the warming level of interest. Target global mean surface temperatures are indicated by the horizontal red lines.

Source: WRI authors.

Table 2 | **Center-point years for each global warming scenario**

MODEL	+1.5°C	+2.0°C	+3.0°C
MIROC-ES2L	2019	2035	2055
UKESM1-0-LL	2015	2024	2034
EC-Earth3-Veg-LR	2015	2024	2060
GFDL-ESM4	2018	2031	2053
INM-CM5-0	2032	2044	2086
MRI-ESM2-0	2018	2024	2048
FGOALS-g3	2020	2025	2068
IPSL-CM6A-LR	2021	2029	2042
CanESM5	2017	2022	2028

Note: Center-point years are the years on which, roughly, the model's global mean surface temperature first exceeds 1.5°C , 2.0°C , or 3.0°C above the 1880–1900 baseline. All indicator values in this study were calculated using model outputs from the 10-year windows approximately centered on the center-point years.

Source: WRI Authors.

Hazards

In this paper, we use *climate hazard* to mean a defined meteorological condition that without mitigation causes or exacerbates a negative societal impact. We chose 10 climate hazards based primarily on temperature and 4 based on precipitation. (One temperature hazard also uses relative humidity.) We selected hazard definitions based on relevance to public health, infrastructure, and economic productivity; interviews and other engagements with local governments; and the authors' general knowledge of the data needs of local governments for climate adaptation planning. The city engagements include interviews with the governments of Hobart, Australia; Makati, Philippines; Tópaga, Colombia; and Vitacura, Chile, conducted in 2021 in collaboration with the Global Covenant of Mayors for Climate and Energy for a pilot adaptation-data project. The interviews focused on which climate hazards were of concern and what role hazard projections might play in planning. We also engaged with the government of Campinas, Brazil, as part of a World Resources Institute partnership with Campinas focused on climate action planning. In this project we worked with the

Campinas government to identify and define climate hazard indicators. In general in the present project, we chose hazards whose indicator calculations were simple but demonstrative of our methods' capabilities and which addressed a variety of hazards relevant to public health, infrastructure maintenance, and economic productivity.

It is useful to note that this project addresses climate hazards only. It does not address how cities differ in their vulnerability (due to demographic, socioeconomic, or geographic factors unrelated to climate) or their ability to tolerate or adapt to climate extremes. (See Begum et al. 2022, particularly Figure 1.5 and discussion thereof, for a more complete treatment of the interplay of hazard, vulnerability, and exposure.) Furthermore, the climate hazards we deal with are limited to those whose definitions include air temperature, precipitation, and, in the case of one hazard, humidity. Because of limitations in the climate simulations that we used, wind, shade, and the direct effects of solar radiation are not included in these hazards. Nothing in our methods would preclude inclusion of these variables in future work if appropriate models and historical data become available.

Maximum annual temperature (Tmax_highest)

Extremely high temperatures can cause illness in humans (Lin et al. 2009) and damage transportation and energy infrastructure (Underwood et al. 2017; Burillo et al. 2019). It is therefore useful for health and engineering departments to know both average values of this hazard and probabilities of temperature extremes reaching particular asset-specific thresholds. The hazard *Tmax_highest* is the highest temperature in a single year.

We calculate this hazard as the maximum value of T_{max} in a calendar year, where T_{max} is the maximum daily air temperature at a height of two meters. We report magnitudes in degrees Celsius.

Days-hotter-than-threshold hazards

Extreme heat is associated with increased morbidity and mortality (Mathes et al. 2017; Green et al. 2019; Khatana et al. 2022), decreased economic activity (Morrissey et al. 2021; Zhao et al. 2021), and increased energy expenditure (Auffhammer and Mansur 2014; Zhang et al. 2022). The hazards *Tmax95pctl_days*, *Tmax35_days*, and *Tmax40_days* all describe the number of days in a year on which the high temperature equals or exceeds a threshold. The definitions we use do not consider humidity, which would exacerbate the health and economic harms of these hazards.

Annual days with maximum temperature equal to or exceeding the 95th percentile (Tmax95pctl_days)

The threshold for *Tmax95pctl_days* is the local 95th percentile of daily high temperature for that city, calculated from the 40-year period 1980–2019. We used this interval because it includes the earliest years available in our observed-climate data set, ERA5, as stored as daily aggregates in Google Earth Engine. A hazard pegged to a locally defined extreme is useful because many negative impacts of temperature are associated with deviations from local norms (Medina-Ramón and Schwartz 2007; Lee et al. 2014).

We calculated this hazard as the number of days in a calendar year on which T_{max} equals or exceeds the local 95th percentile of T_{max}.

Annual days with maximum temperature equal to or exceeding 35°C (*Tmax35_days*)

Similar to *Tmax95pctl_days*, the hazard *Tmax35_days* is the number of days in a year on which the high temperature equals or exceeds 35°C. This temperature is commonly accepted as a human-tolerance threshold because extended exposure to a humid environment at 35°C is likely lethal (Sherwood and Huber 2010). The number of days with dangerously high temperatures is relevant not only for public health but also for economic productivity because outdoor labor and occupancy of uncooled buildings become dangerous.

We calculated this hazard as the number of days in a calendar year on which T_{max} equals or exceeds 35°C.

Annual days with maximum temperature equal to or exceeding 40°C (Tmax40_days)

Similar to *Tmax35_days*, the hazard *Tmax40_days* is the number of days in a year on which the high temperature equals or exceeds 40°C. This temperature was chosen as a critical temperature for infrastructure operation because it is a standard maximum-rated outdoor ambient temperature for electrical transformers (IEEE 2012; IEC 2018).

We calculated this hazard as the number of days in a calendar year on which T_{max} equals or exceeds 40°C.

Annual cooling degree-days (CDD21)

The demand for the cooling of buildings is directly related to cooling degree-days (CDDs; De Rosa 2015), a commonly used hazard based on deviations above a reference temperature.

Numerous studies have used CDDs to model the relationship between temperature regime and demand for cooling (e.g., Jiang et al. 2009; Petri and Caldeira 2015; Andrade et al. 2021; Ukey and Rai 2021). For this hazard, we used 21°C as the reference temperature because recent country-level work by Scoccimarro et al. (2023) predicts widespread increases in CDD21.

We calculated this hazard as

$$CDD21 = \sum_{day} \max(0, T_{avg} - 21°C)$$

where the sum is over the days in the calendar year, and T_{avg} is the respective day's mean air temperature at two-meter height. Our data set presents CDD21 as this absolute quantity, but local differences in the prevalence and energy efficiency of cooling technology make it difficult to reach energy-consumption conclusions based on comparisons of raw CDD values among cities. There is no universal conversion coefficient that maps CDDs to, say, joules.

Annual days with wet-bulb temperature equal to or exceeding 31°C (Twb31_days)

Wet-bulb temperature, T_{wb}, is a thermal-comfort measure that takes into account both air temperature and the evaporative cooling effects of humidity. It differs from wet-bulb globe temperature in that T_{wb} does not consider the effects of wind or shade. Extended exposure to T_{wb} greater than 30°C–31°C can lead to heat-related illness and possibly death (Vecellio et al. 2022).

The advantage of T_{wb} over wet-bulb globe temperature is that it can easily be estimated from commonly measured and modeled meteorological variables. We calculate T_{wb} using the formula of Stull (2011):

$$T_w = T \cdot \arctan\left[0.151977(RH + 8.313659)^{\frac{1}{2}}\right] + \arctan(T + RH) - \arctan(RH - 1.676311) + 0.00391838 \cdot RH^{\frac{3}{2}} \cdot \arctan(0.023101RH) - 4.686035$$

where RH is relative humidity expressed as a percent (e.g., "65" for "65 percent humidity") and is reported in the NEX-GDDP-CMIP6 models. T is air temperature. For T we used T_{max}. The hazard is the number of days on which T_{wb} equals or exceeds 31°C.

Heat waves

Heat waves are periods of abnormally hot weather (Möller et al. 2022). Precise definitions differ with context, with different studies specifying different thresholds for "hot," different minimum durations of the "period," and different temperature variables (i.e., maximum, minimum, or average daily temperature or else a thermal-comfort hazard such as wet-bulb temperature). Heat waves, in general, are associated with increases in mortality (Anderson and Bell 2011; Ragettli et al. 2017; Faurie et al. 2022), though the magnitude of the increase depends on the definition of heat wave used (Xu et al. 2016). For this study, we define heat waves as three or more consecutive days on which the high temperature equals or exceeds the local 90th percentile for daily maximum temperature. This definition allowed us to apply a consistent global definition while accommodating variation in adaptation and acclimation to high temperatures. Xu et al. (2016) suggest the 90th percentile as a compromise between setting too high a threshold and missing some dangerous events and setting too low a threshold and flagging events that might not warrant alarm. We calculated percentiles from the 40-year period 1980–2019.

Because our method calculates hazard magnitudes by the year, for this hazard and other summertime hazards that are defined by runs of consecutive days meeting a particular condition, it is possible we inadvertently divided a single run into two runs at the boundary between two years. To reduce the chance that this occurs, for southern hemisphere cities, where summer spans the calendar-year boundary, we followed common practice and used the year July 1–June 30 to place the summer season within the modeled year (Wehrli et al. 2019; Graw et al. 2020). For northern hemisphere cities, we simply used the calendar year. However, this practice would not be effective in aseasonal environments.

ANNUAL LONGEST HEAT WAVE DURATION (heatwave_duration)

We calculated this hazard as the length in days of the longest heat wave in a year. We defined a heat wave as three or more consecutive days on which the high temperature equals or exceeds the local 90th percentile for daily maximum temperature. For northern hemisphere cities, we used the calendar year. For southern hemisphere cities, we used the year July 1–June 30.

ANNUAL HEAT WAVE COUNT (heatwave_count)

We calculated this hazard as the number of distinct heat waves in a year. We defined a heat wave as three or more consecutive days on which the high temperature equals or exceeds the local 90th percentile for daily maximum temperature. For northern hemisphere cities, we used the calendar year. For southern hemisphere cities, we used the year July 1–June 30.

Annual number of days with average temperature optimal for malaria transmission (malaria_days)

Prevalence of malaria depends importantly on the environmental conditions for its transmission vector, mosquitoes of the genus *Anopheles* (Paaijmans et al. 2009; Blanford et al. 2013). Several studies (e.g., Mordecai et al. 2013; Lunde et al. 2016; Mordecai et al. 2016) have estimated either thermal tolerance ranges or optimal temperature ranges for Anopheles. For this hazard, we adopted the optimal transmission range used by Ryan et al. (2020): 22.9°C–27.8°C. We chose to use this study's range because Ryan et al. used a conservative approach that yielded empirically plausible geographic ranges for *Anopheles gambiae*. Their approach was similar to ours in attempting to project malaria risk ranges based on climate models. Mosquito life cycles, however, depend on more than temperature. This hazard definition is best interpreted as reflecting mosquito activity when there is no mitigation and other conditions exist in which mosquitoes thrive.

We calculated this hazard as the number of days in a calendar year, possibly nonconsecutive, on which 22.9°C ≤ T_{avg} ≤ 27.8°C, where T_{avg} is the daily mean air temperature at two-meter height.

Annual number of days with average temperature optimal for arbovirus transmission (arbovirus_days)

As with malaria transmission, transmission of arboviral diseases such as dengue, chikungunya, and Zika is strongly influenced by air temperature (Mordecai et al. 2017; Ciota and Keyel 2019; Wimberly et al. 2020). For this hazard, we use the optimal temperature range for the vector mosquito *Aedes aegypti* and *Aedes albopictus* as reported in Mordecai et al. (2017): 26°C–29°C. Mordecai et al. base this range on theoretical and laboratory research grounds, and they find that predictions from the range align with epidemiological data.

We calculated this hazard as the number of days in a calendar year on which 26°C ≤ T_{avg} ≤ 29°C, where T_{avg} is the daily mean air temperature at two-meter height.

Heavy one-day precipitation

The risk that an extreme precipitation event overwhelms a city's stormwater management system depends on the climate and on the stormwater system's design parameters (Malik and James 2007; Rosenberg et al. 2010). Precipitation events that exceed design capacity can cause flooding and sewage overflows. Design capacity varies from location to location and is generally based on locally determined extreme precipitation volumes.

Hazards defined by return periods of multiday heavy rain events are probably more directly relevant to the infrastructure impacts of extreme precipitation, but a hazard based on one-day precipitation is computationally less costly and therefore more practical for this global study. Also note that we only calculate precipitation within the pixel whose centroid is the closest to the city centroid, even though precipitation in nearby pixels can also impact flooding. We believe pr_highest and pr90octl_days to be useful for among-city comparisons, but single-location studies for engineering should consider hazards informed by detailed local hydrological models. We do not currently account for whether the precipitation is frozen or liquid, and cities that receive large volumes of snow might find this hazard to be less useful. Estimation of snow and ice volumes is a topic for future iterations of this research.

HIGHEST ANNUAL ONE-DAY PRECIPITATION (pr_highest)

We calculated this hazard as the highest one-day precipitation in a calendar year. We report these hazard magnitudes in millimeters per day.

ANNUAL DAYS WITH ONE-DAY PRECIPITATION EQUAL TO OR EXCEEDING THE 90TH PERCENTILE (pr90pctl_days)

We calculated this hazard as the number of days in a calendar year during which one-day precipitation equals or exceeds the local 90th percentile of one-day precipitation. Percentiles were calculated from the 40-year period 1980–2019. The precipitation is frozen or liquid.

ANNUAL DAYS IN DROUGHT (drought_days)

Droughts have enormous impacts on a city's public health (Stanke et al. 2013; Zhang et al 2019; Sugg et al. 2020) and economy (Desbureaux and Rodella 2019; Cremades et al. 2021). There is no universal definition of drought, and drought concepts can incorporate climate, surface and subsurface hydrology, and the economics and politics of water management. For this hazard, we used the Standardized Precipitation Index (SPI; Svoboda et al. 2012), a widely accepted index adopted by the World Meteorological Organization for the monitoring of meteorological drought.

The SPI fits local, historical precipitation data to a gamma distribution probability model, which is then transformed into a Normal distribution. For the year of interest, precipitation data are mapped onto the Normal distribution, and the SPI reports deviations for each day from the historical mean in standard

deviations. Common SPI values range from –2.5 to 2.5, with negative values representing below-median precipitation. For this hazard, we counted drought days as those with SPI less than –1.5 (McKee et al. 1993, Lloyd-Hughes and Saunders 2002).

We calculated this hazard using the SPI function in the SPEI Python library (Vonk 2023). The hazard is the number of days in a year with SPI less than –1.5. For locations in the southern hemisphere, we used the year July 1–June 30.

For some cities, the SPI function was unable to converge on a usable reference probability distribution. The data set reports no data in these cases.

Annual days with high landslide risk (landsliderisk_days)

Landslides have enormous impacts on cities, both economically and in loss of life (Schuster and Highland 2007; Petley 2009; Mia et al. 2015; Klose et al. 2016). Landslide risk occurs in susceptible areas when there is risk of either earthquake or extended periods of heavy rain. Stanley and Kirschbaum (2017) mapped global landslide susceptibility based on the presence of roads, the absence of trees, proximity to a major tectonic fault, and steep slopes. Kirschbaum and Stanley (2018) combine this susceptibility map with an antecedent rainfall index (ARI), which is an indicator of prolonged, heavy rain. ARI for a particular day, d_0, is calculated as

$$ARI = \frac{\sum_{t=0}^{6} p_t w_t}{\sum_{t=0}^{6} w_t}$$

where t is the number of days before the day of interest, p_t is precipitation on day $d_0 - t$, and $w_t = (t + 1)^{-2}$.

The landslide susceptibility map is available from the Landslide Hazard Assessment for Situational Awareness project, version 1.1.[2] We used this map and intersected it with GHSL's city boundaries to find which of our 996 cities include land with high susceptibility. For the 427 susceptible cities, we then calculated the *landsliderisk_days* hazard as the number of days in a calendar year on which ARI exceeds the local 95th percentile for ARI.

Calculation of average indicator values

For each hazard, we calculated two types of indicators for each location. The first indicator is the **expected hazard value** associated with the GMST of interest. For example, for the indicator *drought_days*, an average value of 8.5 indicates that our estimate of the average number of annual drought days at the GMST of interest is 8.5 days for a particular city. We report this estimate of the expected value as well as a standard deviation of that estimate. (The accuracy of the estimate depends on the accuracy of the underlying model, and the uncertainty reflected in the standard deviation does not include uncertainty in model accuracy.)

The second indicator is the **probability that the hazard value exceeds a particular threshold magnitude** in any year during the 10-year window associated with the GMST of interest. For each hazard, we selected three hazard magnitudes to be used for all three GMSTs, for all locations. The thresholds were selected to serve as a basis for comparisons among GMSTs and among locations rather than for any operational significance. However, these methods could be applied to calculate the probability of exceedance for any locally important thresholds for these indicators, which may be valuable for engineering and risk management applications (Figueiredo et al. 2018). Table 3 lists the magnitude thresholds used for our threshold exceedance probability calculations.

Table 3 | **Hazard-value magnitudes used to calculate threshold exceedance probabilities**

	THRESHOLD MAGNITUDES		
Tmax_highest (°C)	35	40	45
Tmax95pctl_days (days)	60	70	80
Tmax40_days (days)	10	20	30
Tmax35_days (days)	10	20	30
CDD21 (degree-days)	2,000	3,000	4,000
Twb31_days (days)	10	25	30
heatwave_duration (days)	20	30	40
heatwave_count (heat waves)	1	3	5
malaria_days (days)	30	60	90
arbovirus_days (days)	30	60	90
pr_highest (mm)	500	1,000	2,000
pr90pctl_days (days)	20	30	40
drought_days (days)	100	140	180
landsliderisk_days (days)	5	10	20

Source: WRI Authors.

All indicator calculations involved several steps, applied separately for each indicator, for each city location, for each of the three GMSTs of interest. The model grid cell used in the calculations was the cell that contains the city's centroid. The methods for model selection and calibration and to calculate projected averages of hazard magnitudes and of threshold exceedance probabilities are detailed in Wong and Switzer (2023).

1. For each hazard, we selected the three models whose simulated historical values most closely match observed historical values based on RMSD between modeled and observed seasonal means. The meteorological variables used for these comparisons were those used to calculate hazard magnitudes. For example, our heat wave definition uses daily maximum temperature, so model selection was based on daily maximum temperature. For multivariable hazards, we based comparisons on the hazard magnitudes themselves. For historical observations, we used 1980–2014 data from ERA5.
2. All models have their particular biases. We used historical data to reduce these biases. We used ERA5 data to generate a calibration function for each of the three selected models. Each calibration function was based on a percentile-percentile plot (P-P plot) so that the marginal frequency distribution of the calibrated model data approximately matches the marginal frequency distribution of the corresponding ERA5 data. Each model had its own calibration function for each meteorological variable for each location. See Holmgren (1995) for a detailed treatment of P-P plots and their application to model calibration.
3. For each model, using the appropriate calibration function to shift the simulated data, we found for each GMST of interest the 10-year window centered on the GMST exceedance year in Table 2. From the model outputs in the window, we then constructed a histogram of annual hazard indicator values for the relevant 10-year future window (hereafter referred to as a frequency vector) of hazard values. The model outputs are from the model's SSP2-4.5 run as stored in Google Earth Engine. For years before the SSP run begins, we used the model's simulated historical data.
4. We used these frequency vectors to parameterize Bayesian probability models for the frequency of various hazard magnitudes that a city could expect under a particular warming scenario. We used these probability models to generate predictions of the average values of the hazard magnitudes for each scenario.[3] The accompanying data set provides these estimated averages and the standard deviations.
5. To calculate threshold exceedance probabilities, we similarly generated probability models from the frequencies of threshold exceedance found in the simulations.[4] These probability models generate predictive distributions of the exceedance probabilities. We report as estimated probability of threshold-exceedance the means of these distributions, along with the standard deviations of the distributions.

Unlike the standard deviations reported in Tables 6 and 7, the standard deviations reported in the data set and in Tables 4 and 5 describe the uncertainty in the estimate of each indicator. They do not reflect among-city or interannual variability.

RESULTS

In this note we do not summarize the threshold exceedance probability indicators in the data set, but to illustrate how these data are structured we have extracted the exceedance probabilities for the *heatwave_count* hazard for Kigali, Rwanda. Table 4 shows the estimated probabilities that Kigali experiences at least one, three, or five heat waves in one year, for the recent historical reference period 1995–2014 and the three GMSTs. Estimates are provided for all three models selected for temperature hazards in Kigali: FGOALS-g3, INM-CM5-0, and CanESM5. As in the data set, the reported standard deviations describe uncertainty in our estimate, not interannual variability.

The data set reports indicator estimates from each of the three best (i.e., smallest historical RMSD with ERA5) models for each location-hazard combination. Table 5 shows an example from the data set: means and standard deviations of the estimates of the estimated number of heat waves in Kigali, calculated from all three models.

Table 4 | **Probabilities that annual heat waves number exceeds 1, 3, or 5 in Kigali, Rwanda**

	MODEL RANK	RECENT HISTORICAL	+1.5°C	+2.0°C	+3.0°C
1 heat wave	1	36.4 (5.1)	37.1 (5.1)	37.5 (5.2)	38.1 (5.2)
	2	39.4 (23.0)	54.8 (29.3)	62.8 (30.6)	78.7 (40.1)
	3	8.2 (21.4)	10.5 (24.4)	11.9 (26.0)	14.3 (29.8)
3 heat waves	1	31.9 (48.7)	37.3 (51.5)	37.3 (51.5)	47.8 (60.2)
	2	1,101.9 (848.4)	1,242.9 (905.5)	1,305.9 (932.1)	1,436.6 (987.7)
	3	0.2 (2.7)	0.3 (3.7)	0.3 (4.3)	0.5 (5.5)
5 heat waves	1	14.2 (21.1)	20.7 (29.7)	23.5 (29.4)	30.5 (35.7)
	2	4.5 (1.4)	5.7 (1.8)	6.3 (2.0)	7.1 (2.9)
	3	115.1 (98.6)	108.9 (90.0)	106.6 (86.5)	98.8 (77.9)

Note: Probabilities are mean estimates that the annual heat wave number equals or exceeds the threshold. Numbers in parentheses are standard deviations of the predictive distributions generated by the probability models. They therefore describe uncertainty of the estimates, rather than predicted interannual variation. Recent historical values are averages from the 1995–2014 reference period. Models are ranked 1, 2, and 3 based on lowest RMSD of quarterly mean maximum temperatures against ERA5 are FGOALS-g3, INM-CM5-0, and CanESM5, respectively..

Source: WRI Authors.

Table 5 | **Expected number of heat waves for each model for Kigali, Rwanda**

MODEL RANK	RECENT HISTORICAL	+1.5°C	+2.0°C	+3.0°C
1	3.3 (1.0)	4.8 (1.4)	4.9 (1.5)	8.9 (2.3)
2	3.9 (1.1)	4.3 (0.8)	5.8 (1.0)	8.5 (1.2)
3	4.3 (1.4)	5.1 (1.2)	5.5 (1.1)	7.5 (1.4)

Note: Expected values are mean estimates of the expected value of annual heat wave number. Numbers in parentheses are standard deviations of the predictive distributions generated by the probability models. They therefore describe uncertainty of the estimates, rather than predicted interannual variation. Recent historical values are averages from the 1995–2014 reference period. Models ranked 1, 2, and 3 are FGOALS-g3, INM-CM5-0, and CanESM5, respectively.

Source: WRI Authors.

The standard deviation of the three estimates can describe the variation among the estimates from the three models, or the among-model variation. Table 6 shows the all-city average of this standard deviation. In general the average among-model variation increases with increasing GMST. The variation is notably large for the wetbulb-temperature hazard *Twb31_days* and the drought hazard *droughtrisk_days*. For these and all hazards, these standard deviations are useful in that they show substantial differences for some of the indicators among the three best models. The standard deviations are the greatest for most indicators at +3 degrees C above the preindustrial baseline.

The analyses that follow are based only on the projections from the single best of the three selected for each hazard for each location. We remind and urge readers who are interested in understanding the uncertainty of our estimates to compare projections among all three models.

Table 7 shows the means of the city-specific estimates under each warming scenario, taken over all 996 cities. In general, the temperature-based indicators show consistent increases across all cities, but increases and decreases are mixed for the precipitation-based indicators. To calculate population-weighted values, we used the 2020 gridded population estimates from the GHSL GHS-POP data set (Schiavina et al. 2023), which we summed over the metropolitan area polygons in the GHSL Urban Centre Database (Florczyk et al. 2019). Table 8 lists the population-weighted values. Tables 7 and 8 also report standard deviations, which describe the among-city variation in the indicator values.[5] The standard deviations reflect only the uncertainty in our indicator calculations, not the uncertainty in the population data.

Table 6 | **Population-weighted mean values of city-average climate hazard indicator values**

	RECENT HISTORICAL	+1.5°C	+2.0°C	+3.0°C
Tmax_highest	0.50	0.54	0.53	0.60
Tmax95pctl_days	7.62	9.18	11.78	12.70
Tmax40_days	2.55	2.64	3.27	3.59
Tmax35_days	3.71	4.86	5.33	6.50
CDD21	40.09	51.78	52.36	56.19
Twb31_days	9.30	71.62	71.85	72.28
heatwave_duration	6.14	8.41	11.08	11.84
heatwave_count	0.77	0.88	1.00	1.12
malaria_days	7.63	8.86	9.20	10.04
arbovirus_days	7.82	9.06	10.12	10.83
pr_highest	6.57	7.03	7.12	7.07
pr90pctl_days	5.29	5.92	5.96	6.54
drought_days	15.98	17.33	17.34	18.87
landsliderisk_days	4.05	4.08	4.42	4.24

Notes: For each city, we calculated indicators using the three best NEX-GDDP-CMIP6 models based on minimizing RMSD with ERA5. Variation among the results from the three models can be characterized by a standard deviation. This table reports the average across all 996 cities of these standard deviations. The three best models differ from city to city. Larger values reflect greater among-model variation. Recent historical values are averages from the 1995–2014 reference period.

Source: WRI Authors.

Table 7 | **Unweighted all-city average climate hazard indicator values**

	RECENT HISTORICAL	+1.5°C	+2.0°C	+3.0°C
Tmax_highest	36.4 (5.1)	36.6 (5.1)	36.9 (5.1)	37.6 (5.1)
Tmax95pctl_days	39.4 (23.0)	44.2 (25.8)	49.8 (26.9)	65.2 (32.4)
Tmax40_days	8.2 (21.4)	8.8 (22.4)	9.6 (23.3)	12.3 (26.4)
Tmax35_days	31.9 (48.7)	33.0 (49.3)	35.4 (51.1)	42.2 (55.2)
CDD21	1,101.9 (848.4)	1,045.1 (866.0)	1,116.0 (942.1)	1,340.0 (931.0)
Twb31_days	0. (2.7)	0.3 (3.5)	0.3 (4.0)	0.4 (5.1)
heatwave_duration	14.2 (21.1)	16.3 (23.6)	18.4 (26.9)	24.5 (31.9)
heatwave_count	4.5 (1.4)	4.9 (1.6)	5.4 (1.7)	6.4 (2.1)
malaria_days	115.1 (98.6)	114.0 (95.8)	110.4 (91.8)	104.4 (85.1)
arbovirus_days	71.2 (76.0)	74.7 (79.4)	76.9 (81.4)	80.7 (84.9)
pr_highest	40.7 (20.1)	41.7 (20.3)	42.7 (20.5)	43.7 (21.2)
pr90pctl_days	38.7 (12.9)	39.1 (13.4)	40.0 (13.1)	40.6 (13.9)
drought_days	112.4 (50.2)	113.9 (51.6)	114.9 (52.9)	113.6 (51.8)
landsliderisk_days	8.3 (12.0)	20.0 (10.4)	20.8 (10.4)	21.3 (10.9)

Notes: Reported averages are from each city's best model, as assessed by RMSD against ERA5. Parameters for *landsliderisk_days* calculated only for nonzero hazard magnitudes. Calculation of parameters for *droughtrisk_days* excluded no-data instances. Numbers in parentheses are standard deviations, describing among-city variation. The standard deviations are calculated from the predictive distribution from which the mean estimate was calculated. Recent historical values are averages from the 1995–2014 reference period.

Source: WRI Authors.

Table 8 | **Population-weighted all-city average climate hazard indicator values**

	RECENT HISTORICAL	+1.5°C	+2.0°C	+3.0°C
Tmax_highest	36.0 (4.7)	36.2 (4.7)	36.5 (4.7)	37.1 (4.7)
Tmax95pctl_days	38.2 (17.1)	42.6 (19.2)	48.5 (20.0)	63.8 (26.3)
Tmax40_days	6.4 (19.2)	6.8 (20.1)	7.4 (20.6)	9.2 (23.3)
Tmax35_days	25.9 (44.0)	27.2 (44.9)	29.8 (47.2)	35.7 (51.1)
CDD21	1,102.4 (833.5)	1,153.2 (854.1)	1,205.1 (879.5)	1,327.7 (927.7)
Twb31_days	0.1 (2.2)	0.2 (3.2)	0.3 (3.7)	0.4 (4.7)
heatwave_duration	13.3 (15.6)	14.8 (17.2)	16.8 (19.3)	22.6 (23.6)
heatwave_count	4.5 (1.4)	5.0 (1.6)	5.5 (1.6)	6.5 (2.1)
malaria_days	119.7 (99.9)	118.1 (96.1)	113.6 (91.1)	105.4 (82.3)
arbovirus_days	77.9 (81.2)	80.6 (82.7)	83.7 (87.4)	86.9 (91.1)
pr_highest	43.7 (23.3)	45.0 (23.8)	45.4 (22.5)	45.7 (22.8)
pr90pctl_days	39.3 (15.5)	40.0 (15.8)	41.2 (16.90	41.9 (17.0)
drought_days	107.7 (48.8)	108.9 (51.0)	108.1 (52.2)	109.0 (50.9)
landsliderisk_days	11.4 (15.5)	21.3 (14.5)	21.9 (14.7)	22.7 (14.9)

Notes: Reported averages are from each city's best model, as assessed by RMSD against ERA5. Parameters for *landsliderisk_days* calculated only for nonzero hazard magnitudes. Calculation of parameters for *droughtrisk_days* excluded no-data instances. Standard deviations (in parentheses) are calculated with population as frequency weights. Standard deviations reflect only uncertainty in the climate-hazard predictions, not uncertainty in population estimates. The standard deviations are calculated from the predictive distribution from which the mean estimate was calculated. Metropolitan area populations are 2020 estimates from GHS-POP. Recent historical values are averaged over 1995–2014.

Source: WRI Authors.

Some global trends stand out:

- Heat wave duration increases dramatically from +1.5°C to +3.0°C. The unweighted all-city average is 14.2 days for 1995–2014; it increases to 16.3 days at +1.5°C and 24.5 days at +3.0°C. Weighted by 2015 metropolitan area population, the all-city means for *heatwave_duration* at the recent historical reference period, +1.5°C, and +3.0°C are 13.3, 14.8, and 22.6 days, respectively. This means that for the average dweller of our 996 cities, the difference from +1.5°C to +3.0°C brings a 53 percent increase in heat wave duration.
- Heat wave frequency (as captured by *heatwave_count*) also increases, growing from a population-weighted average of 4.5 heat waves per year recently to 5.0 and 6.5 per year, respectively, under +1.5°C and +3.0°C (see Figure 4). Notably, the contrast is starker for cities in low-income countries. The shift from +1.5°C to +3.0°C brings a 29 percent increase in unweighted heat wave frequency for all 996 cities, but it lowers to a 14 percent increase when considering only cities in high-income countries. Cities in low-income countries, in contrast, will see a 45 percent increase in heat wave frequency. Income categories are 2023 categories from the World Bank (n.d.) and are based on gross national income.

Figure 3 | **Change in heat wave frequency between the +1.5°C and +3.0°C warming scenarios**

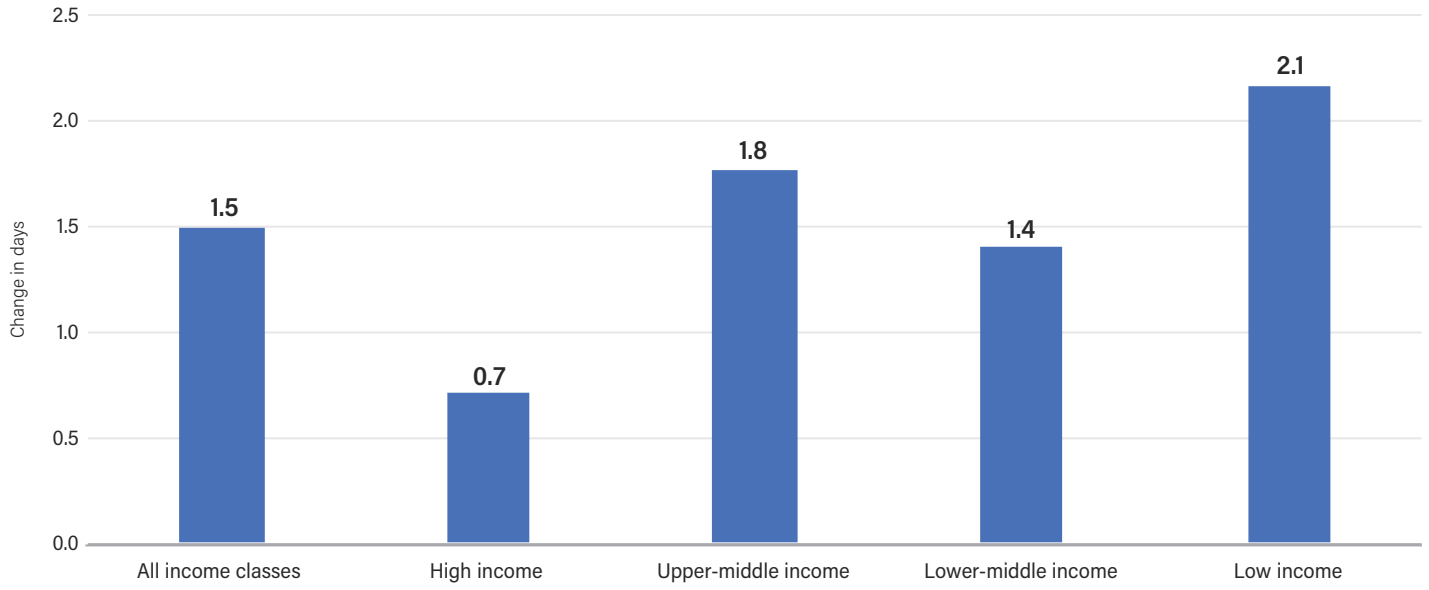

Note: Heat waves become more frequent overall, but the predicted increase is less dramatic for high-income cities and more dramatic for the lowest-income cities.
Source: WRI authors.

There are some regional differences in the direction of change from +1.5˚C to +3.0˚C:

- Using the World Bank's (n.d.) 2023 country-level regional classifications, we find that North America and the Europe–Central Asia region see a modest increase in *malaria_days*, but other locations see a decrease (Figure 4, panel a). Average *arbovirus_days*, in contrast, increase in all regions except the Middle East, East Asia and the Pacific, and South Asia. Across all 996 cities, the average *malaria_days* decrease by 9.6 days whereas average *arbovirus_days* increase by 6.0 days (Figure 4, panel b). By the optimal temperature ranges used in our hazard calculations, arbovirus-carrying mosquitoes thrive at higher temperatures than malaria-carrying mosquitoes. A shift to higher temperatures thus favors arboviral over malarial transmission.
- A shift from +1.5˚C to +3.0˚C brings little change in drought days globally (Figure 5). Cities in all regions see increases or small decreases, except North America, whose average value of *drought_days* decreases by 8.7 days. The Middle East–North Africa region sees a striking increase of 12.1 drought days.

Figure 4 | **Estimated number of days on which average temperature is optimal for disease transmission**

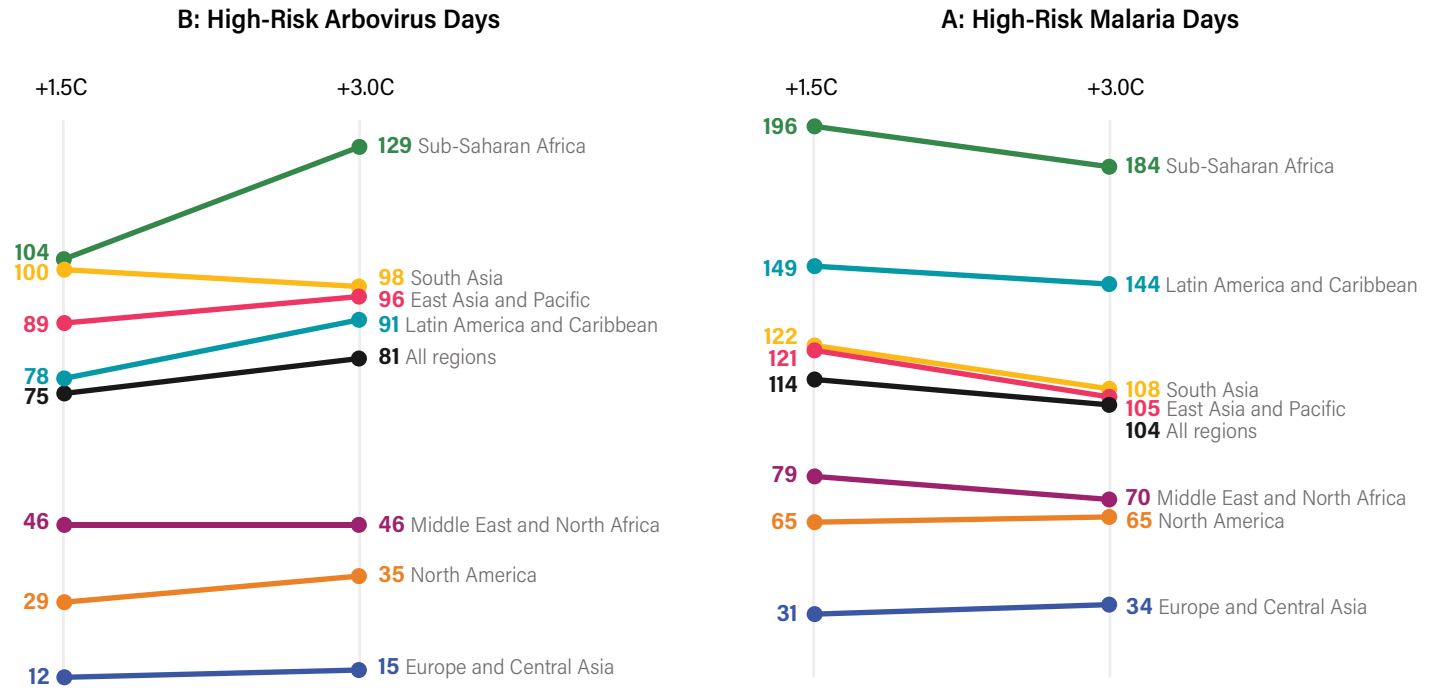

Notes: Panel a shows the malaria-carrying mosquito *Anopheles gambia*, and panel b shows the arbovirus-carrying mosquito *Aedes aegypti*. Days are given for 1.5°C and 3.0°C above the historical baseline.

Source: WRI authors.

Figure 5 | **Change in number of drought days from +1.5°C to +3.0°C of warming**

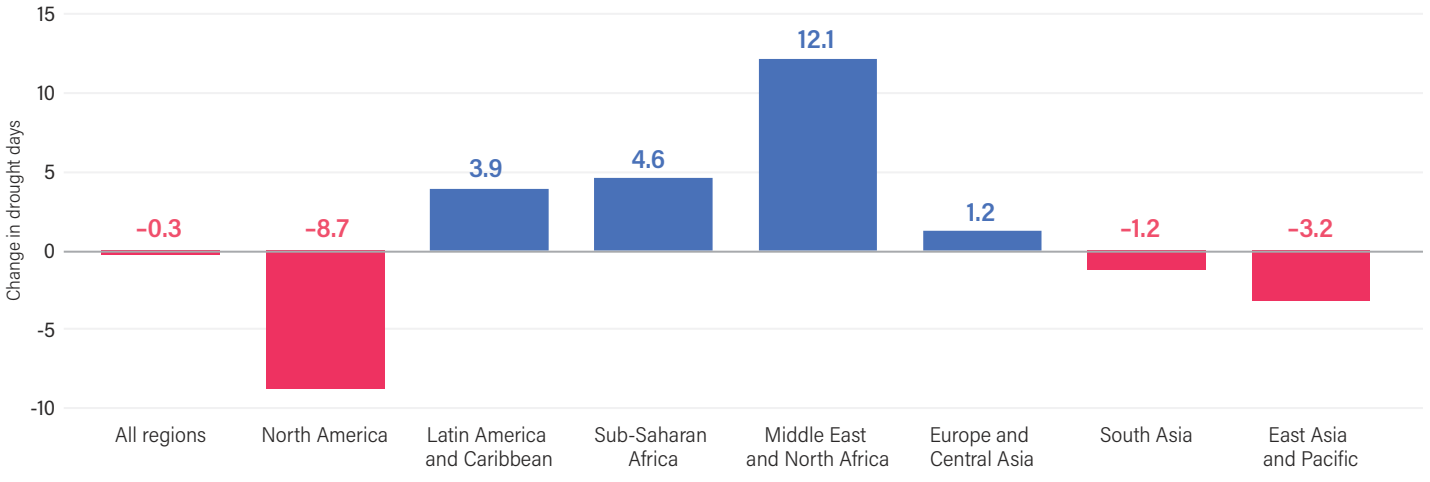

Note: Average drought days changes modestly when averaged across all regions, with a large increase in the Middle East–North Africa region and a large decrease in North America.

Source: WRI authors.

Using the 2020 population estimates (Schiavina et al. 2023), we estimated the number of people exposed to various hazards. Some prominent findings follow:

- Across all 996 cities, at +1.5°C, 547 million people are exposed to 30 or more days with temperatures at or exceeding 35°C. As warming reaches +3.0°C, the number exposed to these temperatures is expected to grow to 701 million.
- Demand for cooling (as captured by CDD21) doubles from the recent historical period 1995–2014 to +1.5°C for 8.7 million people. From the same reference period to +3.0°C, 194 million people have a doubled demand for cooling.

DISCUSSION

The literature associating climate impacts to particular GMST values is vast (e.g., IPCC 2018), but to date there has been little climate-projection work specifically targeting decision-makers in cities. This study fills this gap in two ways: it projects climate hazard magnitudes at a spatial scale appropriate to much city-level decision-making, and it focuses on hazard indicators chosen for relevance to cities.

Our findings are largely unsurprising. Increasing frequency and duration of heatwaves have been observed and predicted by others (Perkins-Kirkpatrick and Gibson 2017, Perkins-Kirkpatrick and Lewis 2020, Qiu and Yan 2020), and Scoccimarro et al. (2023) predicts increasing cooling demand as captured by cooling degree-days. Ryan et al. (2015) predict a contraction of the geographic range of malaria-carrying mosquitos in Africa as the climate warms beyond their physiological tolerance. Mordecai et al. (2020) predict a similar decline in malaria-carrying mosquitos and a surge in arbovirus-carrying mosquitos. Global and regional drought projections vary widely, as drought definitions and models vary widely (Xu et al. 2019, Wang et al. 2021). Studies that, like ours, focused on meteorological drought, and not drought driven by other hydrological processes, have found little evidence for strong directional trends on a global scale, though they acknowledge that drought models that consider evapotranspiration suggest increasing dryness (Asadi Zarch 2022, Vicente-Serrano et al. 2022).

The data we present are suitable to be used for adaptation planning, disaster mitigation, and risk management in cities. We also hope that our work illuminates the particular challenges global warming poses to cities and the need for investment in high-resolution climate models. We also expect that these data can support local activists and subnational political leaders in their work to limit global warming. Additionally, the underlying methods are appropriate for developing many more city- and sector-relevant indicators. We hope that these indicators generate ideas and requests from urban decision-makers for additional indicators to more precisely meet local planning needs.

Limitations

As with all modeling, this study has important limitations. Many of our methodological choices result in simplifications, but, where possible, we made these choices with the intention of keeping our methods conservative—overestimating rather than underestimating uncertainty and underestimating rather than overestimating hazard severity. We note here some important limitations:

- *Our projections include uncertainty.* No attempt to project future trends can eliminate uncertainty. Sources of uncertainty include limitations in the current understanding of earth system processes, uncertainty in future land use and greenhouse gas emissions, uncertainty in our ability to simulate climate computationally, and the stochastic nature of the weather (Kemp et al. 2022). Some uncertainty can be addressed (but not reduced) by the use of more than one climate model. In this project we used nine models, and we present results from three models for each indicator, for each city, in the data set. We urge readers to consult the data from all three models to have a sense of the magnitude of the uncertainty (see below, "Interpreting the data"), but note that even if the models agree perfectly some underlying uncertainty remains.
- *Our models do not consider urban heat islands or other urban climate effects.* The effects of pavement, buildings, and vehicular traffic are not accounted for in global climate models like those included in NEX-GDDP-CMIP6. Particularly in the case of the urban heat island effect, we expect our methods to underestimate the magnitudes of heat-related hazards. (See Phelan et al. [2015] and Deilami et al. [2018] for reviews on urban heat islands.)
- *We do not consider urbanization or other demographic processes.* Cities grow in population and spatial extent over time, but we do not account for these changes in this project. Population changes would likely affect the population-weighted indicators we report in this paper. Spatial-extent changes might occasionally affect which model grid cell is used for indicator calculation, but we do not think the differences are likely to be large. Increasing urbanization and population growth would also likely increase urban heat island effects.

- *Spatial resolution of 0.25 degrees is not sufficiently fine for intra-city work.* Neighborhoods within a city can vary enormously in climate. Numerous factors—building height, vegetation, local topography, proximity to large bodies of water—can influence temperature and precipitation in ways that contribute to within-city differences in hazard exposure and quality of life. In the case of our malaria and arbovirus transmission hazards, the spatial resolution of our data can obscure vector hotspots. Our data does not capture variation at the neighborhood scale and is therefore not useful in understanding neighborhood-level differences in climate adaptation priorities.
- *We probably underestimate variation, especially in precipitation.* Spatially coarse data has the effect of averaging away any variation that exists at finer scales (O'Neill et al. 1986). One consequence of this is that our calculations probably underestimate variation and fail to capture peaks and troughs at fine geographic scales both in the hazard magnitudes and in the hazard indicators.
- *Our exposure estimates are based on recent populations, not population projections.* We use GHSL's 2020 population estimates and GHSL's 2015 estimates of the spatial extents of urban areas. A more robust approach would base exposure estimates on projections both of population and of urban extents, even as it introduces additional uncertainty through inclusion of another projected variable. The result is that future population exposure is underestimated.

Some of these limitations would be mitigated with climate model outputs at finer spatial resolution. For this global study, we used global models and were limited by the resolution of available models. Nothing would preclude a researcher from applying the indicator calculation methods in Wong and Switzer (2023) to outputs from a local climate model with finer resolution.

However, even with limited data availability, we see that a world 3.0°C warmer than the preindustrial baseline is likely to be far worse for far more city dwellers than a world that is only 1.5°C warmer. This is particularly true for heat-related hazards—heat waves become longer and more common, more energy is required to maintain safe and comfortable conditions indoors, and there is greater risk of infrastructure-endangering temperatures. Also, these hazards are not uniformly distributed. Cities in the Global South face disproportionately greater increases in arbovirus risk, and cities in low-income countries are predicted to experience more frequent heat waves. In this paper, we have limited our effort on analysis of socioeconomic disparities in climate hazard exposure and vulnerability. However, the accompanying data set should serve as a sound basis for further work in this area.

Interpreting the data

We expect the indicators in our data set to be useful in a variety of applications, and we acknowledge that some users might be unfamiliar with this sort of data. We offer the following advice on interpreting our, and all, model results.

- *Acknowledge uncertainty.* The data set includes two ways to assess some (but not all: see above, "Limitations") of the uncertainty inherent in our estimates of the indicator values. Each estimate is the mean of the predicted indicator values from a single model. The accompanying standard deviation describes the variation in that model's predictions. Large standard deviations indicate greater *within-model* uncertainty. This is true for both types of indicator—expected value and threshold-exceedance probability. We also provide estimates (and accompanying standard deviations) from three independent climate models. Comparing the three indicator values provides a sense of the uncertainty that arises from differences in modeling methods—*among-model* uncertainty. Greater disagreement among the three models' projections indicates greater uncertainty.
- *Remain mindful of the spatial scale of the indicators.* Our input data, and therefore our indicator estimates, are spatially averaged over grid cells that are 0.25 degrees by 0.25 degrees in size. Near the equator, 0.25 degrees is equivalent to approximately 28 kilometers, so a single grid cell is larger than many cities. This means that for many locations, the averages include both urban climates and climates in outlying areas. One consequence of the averaging is that temperatures experienced in the centers of cities are likely to be higher than the average over its grid cell if that cell also includes rural areas.
- *Avoid combining indicators numerically.* We calculate every indicator independently of the others, and we are aware of no mathematical justification for combining two indicators that have been calculated for different hazards or from different models. For this reason we discourage combining indicators for different hazards. For example, it would not be appropriate to multiply heat wave duration and heat wave frequency to estimate the annual number of days spent in heat waves. Number of days spent in heat waves would define a new hazard, and the methods in Wong and Switzer (2023) could be applied to estimate its future average magnitudes and probabilities of threshold exceedance. We also discourage

reporting across-model indicator means. If a single indicator value is desired, we recommend reporting either the median of the three values or the value from the top-ranked model. The latter has the advantage that any one city's indicators for different GMSTs will be from the same model.

- *Avoid sorting or ranking the data by indicator value.* Users of multi-city data occasionally want to sort the data in order to find the cities with the most extreme indicator values—for example, the cities with the highest projected annual temperatures. We discourage this. Every indicator estimate can be thought of as the sum of a true value (whose value we do not know) and some modeling error. If two cities had the same true number of peak malaria-transmission days at a particular GMST, their *malaria_days* indicator values would almost certainly be different in our data set because of chance error. When data are sorted or ranked by indicator values, values that are high or low because of chance error can be overrepresented in the high or low ranks. The result is that lists of the hottest or driest cities are likely to include cities that, but for chance, would not make the list.
- *Focus on aggregates.* We discourage grouping cities by indicator-value rank, but we encourage other ways of grouping cities. It might be fruitful to compare average indicator values among cities grouped by size, wealth level, geographic region, progress toward climate goals, or any other attribute that is not derived from our data.
- *Avoid overstating impact.* Our intention is to address issues that are salient to the lives and livelihoods of cities, but in this project we have been limited to climatic variables that are straightforward to model. This approach necessarily leaves unaddressed relevant, important factors. For example, our treatment of infectious-disease transmission focuses only on optimal temperatures for the adult mosquitos that carry disease. It does not address climatic factors that affect other parts of the pathogen, vector, or host life cycles. It does not account for whether the pathogens or mosquitos are present to begin with. And it does not address mitigation actions like vaccination and vector control. Similarly, our treatment of drought addresses only rainfall and does not account for important drought factors like groundwater dynamics, evapotranspiration, and water use.
- *Question counterintuitive values.* Some indicators for some cities will inevitably be surprising. For example, some historically cool cities will be characterized as surprisingly hot, or an indicator calculated for +2.0°C is lower in value than both the +1.5°C and 3.0°C values. Without an in-depth study using local data or high-resolution local modeling, it is impossible to know how much of the gap between data and intuition to attribute to a surprising but correct future and how much to attribute to systematic or chance error. It is useful to remember that these data are not the totality of the information we bring to bear; we have knowledge about local context and conditions, as well as prior knowledge of the city's historical climate trends. Our data do not replace existing knowledge, but should rather be evaluated in light of it and—with appropriate caveats—be added to it.

DATA AVAILABILITY

All indicator values, along with summary tables, are available in the provided data set.[6] The spreadsheet containing the indicator values includes mean estimates for each indicator for each of the GMSTs of interest: +1.5°C, +2.0°C, and +3.0°C. They also report recent historical reference period averages, calculated from modeled data for the 20-year period 1995–2014. We also report for each mean estimate the standard deviation of the predictive distribution from which the mean estimate was taken. These are the mean and standard deviation of the predictive distribution of the indicator as generated by a Bayesian probability model. The standard deviation should not be interpreted as reflecting variability of the hazard magnitude but rather an indicator of some of the uncertainty in our estimate of the mean hazard magnitude. Mean estimates of the indicators, and standard deviations, are provided for the three best models for each city as assessed by RMSD against ERA5.

The spreadsheet columns and their values are as follows:

loc_id	An integer unique to each city
city	City name
country	Country name
latitude	Latitude in decimal degrees north
longitude	Longitude in decimal degrees east
hazard	Hazard short-names. Listed in the section "Hazards" and in Table 3.
scenario	Warming scenarios. Can be recent_historical (i.e., 1995–2014), 1.5C, 2.0C, or 3.0C.
model	The NEX-GDDP-CMIP6 model used for calculating the indicator. Models are listed in Table 1.
model_rank	The rank of the model. Can be 1, 2, or 3, where the model with rank 1 has the strongest association between its historical predictions and ERA5 data.

indicator	Can be exceedanceprob (for probability of exceeding the threshold) or expectedvalue (for the expected value of the indicator magnitude).
threshold	Hazard magnitudes chosen as extreme values, listed in Table 3
mean_estimate	The mean of the predictive distribution of indicator values as generated by a Bayesian probability model. This value can be interpreted as an estimate of the indicator value.
stdev_estimate	The standard deviation of the predictive distribution of indicator values as generated by a Bayesian probability model. This value reflects the uncertainty in the estimate of the indicator value.

APPENDIX. SUITABILITY OF NEX-GDDP-CMIP6 FOR URBAN APPLICATIONS.

The CMIP6 models generally do not model urban climate processes. In the absence either of urban-specific climate modeling (e.g., Zhao et al. 2021) or bias correction using empirical city-level data, a CMIP6 model will fail to account for the climate impacts of cities (e.g., heat island effect). The NEX-GDDP-CMIP6 downscaled dataset was calculated using a bias-correction process using the Global Meteorological Forcing Dataset (GMFD) for Land Surface Modeling (Sheffield et al. 2006). We apply a second bias correction to NEX-GDDP-CMIP6 model outputs (see Wong and Switzer [2023] for methodological details) using the European Centre for Medium-Range Weather Forecasts Reanalysis version 5 (ERA5; ECMWF 2022). GMFD and ERA5 are reanalysis datasets: they begin with empirical data and use modeling for bias correction and to fill data gaps. We note that because GMFD and ERA5 include empirical climate observations, urban climates are reflected in the bias-corrected NEX-GDDP-CMIP6 model outputs for urban locations used in this study, even if the underlying CMIP6 models do not explicitly model cities.

The scatterplots in Figure A1 illustrate the relationships among the monthly means of daily maximum temperature data from four datasets for the years 2006–2024. The four datasets are the NEX-GDDP-CMIP6 downscaled data from the CanESM climate model, the same CanESM data modified with an urban climate model by Zhao and colleagues (2021), ERA5, and weather-station data from the Global Historical Climatology Network (GHCN; Lawrimore et al. 2011). The Zhao et al. dataset is the only publicly available dataset that applies urban climate modeling to global climate models. Each scatterplot includes 227,088 points: 12 monthly means × 19 years × 996 cities. The data are the values in the respective datasets at the grid cell or weather station geographically nearest to the city centroid.

Table A1 reports the root mean squared difference (RMSD) between the two model datasets (NEX-GDDP-CMIP6 and the Zhao et al. data) and the two empirical datasets (ERA5 and GHCN). The association between the NEX-GDDP-CMIP6 outputs and the ERA5 data is remarkably strong, as can be seen in the small RMSD value (2.27) and the narrow point cloud in the nex-ERA5 scatterplot in Figure 2. The Zhao et al. data outperform NEX-GDDP-CMIP6 in their association with the GHCN weather-station data, but the difference as quantified by RMSD is small.

The strong association between the NEX-GDDP-CMIP6 CESM temperature data and ERA5 temperature data suggests that NEX-GDDP-CMIP6 is suitable for predicting climate at a spatial resolution similar to the ERA5 resolution (31 km). The weaker association with the GHCN weather-station data suggests that NEX-GDDP-CMIP6 is less suitable for predicting climate at point locations. This contrast underscores an important caveat about our research: the indicator values we report are spatial averages over grid cells that are 0.25 degrees by 0.25 degrees in extent. They should not be interpreted as estimates for cities as point locations.

Figure A1 | **Dataset comparisons for monthly means of daily maximum temperature, 2006–2024**

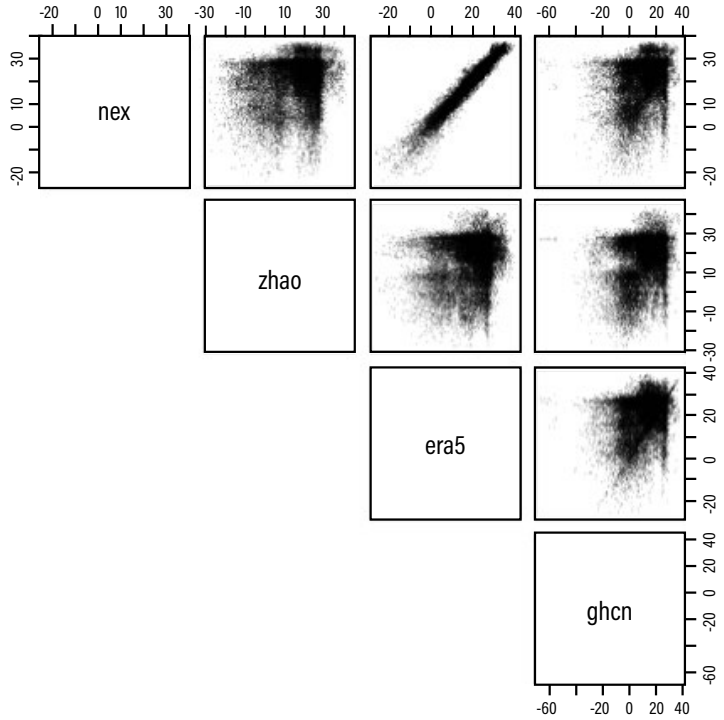

Notes: The datasets compared are the CanESM model outputs in NEX-GDDP-CMIP6 ("nex"), the CanESM model outputs as modified with urban climate modeling by Zhao et al. ("zhao"), the ERA5 reanalysis dataset, and weather station data from the Global Historical Climatology Network ("ghcn"). The points represent monthly mean of daily maximum temperature, 2006–2024, in the 996 study cities. The unit for all axes is degrees Celsius.

Source: WRI authors.

Table A1 | **Root-mean-squared differences between modeled and empirical temperature data**

	ERAS	GHCN
NEX-GDDP-CMIP6	2.27	15.73
Zhao et al.	13.68	14.94

Notes: The datasets compared are the CESM model outputs in NEX-GDDP-CMIP6, the CESM model outputs as modified with urban climate modeling by Zhao et al., the ERA5 reanalysis dataset, and weather station data from the Global Historical Climatology Network. Compared data are monthly means of daily maximum temperature, 2006–2024, in the 996 study cities.

Source: WRI Authors.

ENDNOTES

1. The data set can be downloaded at https://datasets.wri.org/dataset/city-scale-climate-hazard-indicators-warming-scenarios.
2. The landslide susceptibility map can be downloaded at https://gpm.nasa.gov/landslides/projects.html.
3. Specifically, we used a noninformative Bayes Dirichlet prior distribution for the histogram of annual climate hazard indicators and conditioned them on the specific frequency vectors. For each model, hazard, and GMST, this yielded a posterior multinomial distribution that characterizes the uncertainty in the histogram of the future indicator values for this period. Samples from this posterior multinomial distribution were used to generate the predictive distribution for the average annual hazard indicator. The means and standard deviations of these predictive distributions are shown as rows in the accompanying data set.
4. For predicted probabilities of threshold exceedance, a Bayes framework was applied to frequencies of threshold exceedance counts in the hazard-value frequency distribution. In the case of the heat wave hazards, samples from a gamma prior were used to parameterize posterior Poisson distributions. For the other hazards, samples from a beta prior were used to parameterize posterior binomial distributions. Samples from the posterior distributions are predictive distributions of the future counts of exceedance events.
5. The means in Tables 8 and 9 are population parameters, rather than sample statistics. The standard deviations should therefore be interpreted only as a measure of among-city variability, and not as an indicator of significant differences from null values.
6. See endnote 1.

REFERENCES

Anderson, G.B., and M.L. Bell. 2011. "Heat Waves in the United States: Mortality Risk during Heat Waves and Effect Modification by Heat Wave Characteristics in 43 US Communities." *Environmental Health Perspectives* 119 (2): 210–18. https://doi.org/10.1289/ehp.1002313.

Andrade, C., S. Mourato, and J. Ramos. 2021. "Heating and Cooling Degree-Days Climate Change Projections for Portugal." *Atmosphere* 12 (6): 715. https://doi.org/10.3390/atmos12060715.

Arnell, N.W., J.A. Lowe, B. Lloyd-Hughes, and T.J. Osborn. 2018. "The Impacts Avoided with a 1.5°C Climate Target: A Global and Regional Assessment." *Climatic Change* 147 (March): 61–76. https://doi.org/10.1007/s10584-017-2115-9.

Asadi Zarch, M.A. 2022. "Past and Future Global Drought Assessment." *Water Resources Management* 36 (13): 5259–76.

Auffhammer, M., and E.T. Mansur. 2014. "Measuring Climatic Impacts on Energy Consumption: A Review of the Empirical Literature." *Energy Economics* 46 (November): 522–30. https://doi.org/10.1016/j.eneco.2014.04.017.

Begum, A., R. Lempert, E. Ali, T.A. Benjaminsen, T. Bernauer, W. Cramer, X. Cui, K. Mach, G. Nagy, N.C. Stenseth, R. Sukumar, and P. Wester. 2022. "Point of Departure and Key Concepts." In *Climate Change 2022: Impacts, Adaptation, and Vulnerability*. Contribution of Working Group II to the Sixth Assessment Report of the Intergovernmental Panel on Climate Change H.-O. Pörtner, D.C. Roberts, M. Tignor, E.S. Poloczanska, K. Mintenbeck, A. Alegría, M. Craig, S. Langsdorf, S. Löschke, V. Möller, A. Okem, B. Rama (eds.). New York and Cambridge: Cambridge University Press, 121–96, doi:10.1017/9781009325844.003.

Blanford, J.I., S. Blanford, R.G. Crane, M.E. Mann, K.P. Paaijmans, K.V. Schreiber, and M.B. Thomas. 2013. "Implications of Temperature Variation for Malaria Parasite Development across Africa." *Scientific Reports* 3 (1300). https://doi.org/10.1038/srep01300.

Burillo, D., M.V. Chester, S. Pincetl, and E. Fournier. 2019. "Electricity Infrastructure Vulnerabilities due to Long-Term Growth and Extreme Heat from Climate Change in Los Angeles County." *Energy Policy* 128 (May): 943–53. https://doi.org/10.1016/j.enpol.2018.12.053.

Ciota, A.T., and A.C. Keyel. 2019. "The Role of Temperature in Transmission of Zoonotic Arboviruses." *Viruses* 11 (11): 1013. https://doi.org/10.3390/v11111013.

Cremades, R., A. Sanchez-Plaza, R.J. Hewitt, H. Mitter, J.A. Baggio, M. Olazabal, A. Broekman, B. Kropf, and N.C. Tudose. 2021. "Guiding Cities under Increased Droughts: The Limits to Sustainable Urban Futures." *Ecological Economics* 189: 107140. https://doi.org/10.1016/j.ecolecon.2021.107140.

Deilami, K., M. Kamruzzaman, and Y. Liu. 2018. "Urban Heat Island Effect: A Systematic Review of Spatio-temporal Factors, Data, Methods, and Mitigation Measures." *International Journal of Applied Earth Observation and Geoinformation* 67 (May): 30–42. https://doi.org/10.1016/j.jag.2017.12.009.

De Rosa, M., V. Bianco, F. Scarpa, and L.A. Tagliafico. 2015. "Historical Trends and Current State of Heating and Cooling Degree-Days in Italy." *Energy Conversion and Management* 90 (January): 323–35. https://doi.org/10.1016/j.enconman.2014.11.022.

Desbureaux, S., and A.-S. Rodella. 2019. "Drought in the City: The Economic Impact of Water Scarcity in Latin American Metropolitan Areas." *World Development* 114 (February): 13–27. https://doi.org/10.1016/j.worlddev.2018.09.026.

Dosio, A., L. Mentaschi, E.M. Fischer, and K. Wyser. 2018. "Extreme Heat Waves under 1.5°C and 2°C Global Warming." *Environmental Research Letters* 13 (April): 054006. https://doi.org/10.1088/1748-9326/aab827.

ECMWF (European Centre for Medium-Range Weather Forecasts). 2022. "ERA5: Data Documentation." July 14. https://confluence.ecmwf.int/display/CKB/ERA5%3A+data+documentation.

Faurie, C., B.M. Varghese, J. Liu, and P. Bi. 2022. "Association between High Temperature and Heatwaves with Heat-Related Illnesses: A Systematic Review and Meta-analysis." *Science of the Total Environment* 852 (December): 158332. https://doi.org/10.1016/j.scitotenv.2022.158332.

Figueiredo, R., M.L. Martina, D.B. Stephenson, and B.D. Youngman. 2018. "A Probabilistic Paradigm for the Parametric Insurance of Natural Hazards." *Risk Analysis* 38 (11): 2400–14. https://doi.org/10.1111/risa.13122.

Florczyk, A., C. Corbane, M. Schiavina, M. Pesaresi, L. Maffenini, M. Melchiorri, P. Politis, et al. 2019. "GHS-UCDB R2019A: GHS Urban Centre Database 2015, Multitemporal and Multidimensional Attributes." European Commission, Joint Research Centre. https://data.jrc.ec.europa.eu/dataset/53473144-b88c-44bc-b4a3-4583ed1f547e.

Gorelick, N., M. Hancher, M. Dixon, S. Ilyushchenko, D. Thau, and R. Moore. 2017. "Google Earth Engine: Planetary-Scale Geospatial Analysis for Everyone." *Remote Sensing of Environment* 202 (December): 18–27. https://doi.org/10.1016/j.rse.2017.06.031.

Graw, V., G. Ghazaryan, J. Schreier, J. Gonzalez, A. Abdel-Hamid, Y. Walz, K. Dall, J. Post, A. Jordaan, and O. Dubovyk. 2020. "Timing Is Everything—Drought Classification for Risk Assessment." *IEEE Journal of Selected Topics in Applied Earth Observations and Remote Sensing* 13: 428–33. https://doi.org/10.1109/JSTARS.2019.2963576.

Green, H., J. Bailey, L. Schwarz, J. Vanos, K. Ebi, and T. Benmarhnia. 2019. "Impact of Heat on Mortality and Morbidity in Low and Middle Income Countries: A Review of the Epidemiological Evidence and Considerations for Future Research." *Environmental Research* 171 (April): 80–91. https://doi.org/10.1016/j.envres.2019.01.010.

Holmgren, E.B. 1995. "The P-P Plot as a Method for Comparing Treatment Effects." *Journal of the American Statistical Association* 90 (429) 360–65. https://doi.org/10.1080/01621459.1995.10476520.

IEC (International Electrotechnical Commission). 2018. "IEC 60076-7:2018: Power Transformers—Part 7: Loading Guide for Mineral-Oil-Immersed Power Transformers." https://webstore.iec.ch/publication/34351.

IEEE (Institute of Electrical and Electronics Engineers). 2012. "IEEE C57.91-2011: IEEE Guide for Loading Mineral-Oil-Immersed Transformers and Step-Voltage Regulators." https://standards.ieee.org/ieee/C57.91/5297/.

IPCC (Intergovernmental Panel on Climate Change). 2018. *Global Warming of 1.5°C. An IPCC Special Report on the Impacts of Global Warming of 1.5°C above Pre-industrial Levels and Related Global Greenhouse Gas Emission Pathways, in the Context of Strengthening the Global Response to the Threat of Climate Change, Sustainable Development, and Efforts to Eradicate Poverty*. Edited by V. Masson-Delmotte, P. Zhai, H.-O. Pörtner, D. Roberts, J. Skea, P.R. Shukla, A. Pirani, et al. Cambridge and New York: Cambridge University Press. https://www.ipcc.ch/sr15/.

Jacob, D., L. Kotova, C. Teichmann, S.P. Sobolowski, R. Vautard, C. Donnelly, A.G. Koutroulis, et al. 2018. "Climate Impacts in Europe Under +1.5°C Global Warming." *Earth's Future* 6 (2): 264–85. https://doi.org/10.1002/2017EF000710.

Jiang, F., X. Li, B. Wei, R. Hu, and Z. Li. 2009. "Observed Trends of Heating and Cooling Degree-Days in Xinjiang Province, China." *Theoretical and Applied Climatology* 97: 349–60. https://doi.org/10.1007/s00704-008-0078-5.

Khatana, S.A.M., R.M. Werner, and P.W. Groeneveld. 2022. "Association of Extreme Heat with All-Cause Mortality in the Contiguous US 2008–2017." *JAMA Network Open* 5 (5): e2212957. https://doi.org/10.1001/jamanetworkopen.2022.12957.

Kemp, L., C. Xu, J. Depledge, K.L. Ebi, G. Gibbins, T.A. Kohler, J. Rockström, M. Scheffer, H.J. Schellnhuber, W. Steffen, and T.M. Lenton. 2022. "Climate Endgame: Exploring Catastrophic Climate Change Scenarios." *Proceedings of the National Academy of Sciences* 119 (34): e2108146119.

Kirschbaum, D., and T. Stanley. 2018. "Satellite-Based Assessment of Rainfall-Triggered Landslide Hazard for Situational Awareness." *Earth's Future* 6 (3): 505–23. https://doi.org/10.1002/2017EF000715.

Klose, M., P. Maurischat, and B. Damm. 2016. "Landslide Impacts in Germany: A Historical and Socioeconomic Perspective." *Landslides* 13 (February): 183–99. https://doi.org/10.1007/s10346-015-0643-9.

Kuma, P., F.A.-M. Bender, and A.R. Jönsson. 2023. "Climate Model Code Genealogy and Its Relation to Climate Feedbacks and Sensitivity." *Journal of Advances in Modeling Earth Systems* 15 (7): e2022MS003588. https://doi.org/10.1029/2022MS003588.

Lawrimore, J.H., M.J. Menne, B.E. Gleason, C.N. Williams, D.B. Wuertz, R.S. Vose, and J. Rennie. 2011. *Global Historical Climatology Network—Monthly (GHCN-M)*, Version 3. NOAA National Centers for Environmental Information. doi:10.7289/V5X34VDR. Accessed 10 July 2024.

Lee, M., F. Nordio, A. Zanobetti, P. Kinney, R. Vautard, and J. Schwartz. 2014. "Acclimatization across Space and Time in the Effects of Temperature on Mortality: A Time-Series Analysis." *Environmental Health* 13 (October): 89. https://doi.org/10.1186/1476-069X-13-89.

Li, K., J. Pan, W. Xiong, W. Xie, and T. Ali. 2022. "The Impact of 1.5°C and 2.0°C Global Warming on Global Maize Production and Trade." *Scientific Reports* 12 (October): 17268. https://doi.org/10.1038/s41598-022-22228-7.

Lin, S., M. Luo, M., R.J. Walker, X. Liu, S.-A. Hwang, and R. Chinery. 2009. "Extreme High Temperatures and Hospital Admissions for Respiratory and Cardiovascular Diseases." *Epidemiology* 20(5): 738–46. https://doi.org/10.1097/EDE.0b013e3181ad5522.

Lloyd-Hughes, B., and M.A. Saunders. 2002. "A Drought Climatology for Europe." *International Journal of Climatology* 22 (13): 1571–92.

Lunde, T.M., M.N. Bayoh, and B. Lindtjørn. 2013. "How Malaria Models Relate Temperature to Malaria Transmission." *Parasites and Vectors* 6 (20). https://doi.org/10.1186/1756-3305-6-20.

Malik, U., and W. James. 2007. "Reliability of Design Storms Used to Size Urban Stormwater System Elements." *Journal of Water Management Modeling* R227-16 (15): 309–26. https://doi.org/10.14796/JWMM.R227-16.

Meinshausen, M., J. Lewis, C. McGlade, J. Gütschow, Z. Nicholls, R. Burdon, L. Cozzi, and B. Hackmann. 2022. "Realization of Paris Agreement Pledges May Limit Warming Just below 2°C." *Nature* 604 (April): 304–9. https://doi.org/10.1038/s41586-022-04553-z.

Mathes, R.W., K. Ito, K. Lane, and T.D. Matte. 2017. "Real-Time Surveillance of Heat-Related Morbidity: Relation to Excess Mortality Associated with Extreme Heat." *PLoS ONE* 12 (9): e0184364. https://doi.org/10.1371/journal.pone.0184364.

McKee, T.B., N.J. Doesken, and J. Kleist. 1993. "The Relationship of Drought Frequency and Duration to Time Scales." *Proceedings of the 8th Conference on Applied Climatology* 17 (22): 179–83.

Mia, M.T., N. Sultana, and A. Paul. 2015. "Studies on the Causes, Impacts and Mitigation Strategies of Landslide in Chittagong City, Bangladesh." *Journal of Environmental Science and Natural Resources* 8 (2): 1–5. https://doi.org/10.3329/jesnr.v8i2.26854.

Millar, R.J., J.S. Fuglestvedt, P. Friedlingstein, J. Rogelj, M.J. Grubb, H.D. Matthews, R.B. Skeie, P.M. Forster, D.J. Frame, and M.R. Allen. 2017. "Emission Budgets and Pathways Consistent with Limiting Warming to 1.5°C." *Nature Geoscience* 10 (October): 741–47. https://doi.org/10.1038/ngeo3031.

Mitchell, D., K. AchutaRao, M. Allen, I. Bethke, U. Beyerle, A. Ciavarella, P.M. Forster, et al. 2017. "Half a Degree Additional Warming, Prognosis and Projected Impacts (HAPPI): Background and Experimental Design." *Geoscientific Model Development* 10 (2): 571–83. https://doi.org/10.5194/gmd-10-571-2017.

Medina-Ramón, M., and J. Schwartz. 2007. "Temperature, Temperature Extremes, and Mortality: A Study of Acclimatization and Effect Modification in 50 United States Cities." *Occupational and Environmental Medicine* 64 (12): 827–33. https://doi.org/10.1136/oem.2007.033175.

Möller, V., R. van Diemen, J.B.R. Matthews, C. Méndez, S. Semenov, J.S. Fuglestvedt, and A. Reisinger, eds. 2022: "Annex II: Glossary." In *Climate Change 2022: Impacts, Adaptation and Vulnerability*. Contribution of Working Group II to the Sixth Assessment Report of the Intergovernmental Panel on Climate Change, edited by H.-O. Pörtner, D.C. Roberts, M. Tignor, E.S. Poloczanska, K. Mintenbeck, A. Alegría, M. Craig, et al. Cambridge and New York: Cambridge University Press. https://doi.org/10.1017/9781009325844.029.

Mordecai, E.A., K.P. Paaijmans, L.R. Johnson, C. Balzer, T. Ben-Horin, E. de Moor, A. McNally, et al. 2012. "Optimal Temperature for Malaria Transmission Is Dramatically Lower than Previously Predicted." *Ecology Letters* 16 (1): 22–30. https://doi.org/10.1111/ele.12015.

Mordecai, E.A., J.M. Cohen, M.V. Evans, P. Gudapati, L.R. Johnson, C.A. Lippi, K. Miazgowicz, et al. 2017. "Detecting the Impact of Temperature on Transmission of Zika, Dengue, and Chikungunya Using Mechanistic Models." *PLoS Neglected Tropical Diseases* 11 (4): e0005568. https://doi.org/10.1371/journal.pntd.0005568.

Mordecai, E.A., S.J. Ryan, J.M. Caldwell, M.M. Shah, and A.D. LaBeaud. 2020. "Climate Change Could Shift Disease Burden from Malaria to Arboviruses in Africa." *Lancet Planetary Health* 4 (9): e416–23. https://doi.org/10.1016/S2542-5196(20)30178-9.

Morrissey, M.C., G.J. Brewer, W.J. Williams, T. Quinn, and D.J. Casa. 2021. "Impact of Occupational Heat Stress on Worker Productivity and Economic Cost." *American Journal of Industrial Medicine* 64 (12): 981–88. https://doi.org/10.1002/ajim.23297.

Nangombe, S., T. Zhou, W. Zhang, B. Wu, S. Hu, L. Zou, and D. Li. 2018. "Record-Breaking Climate Extremes in Africa under Stabilized 1.5°C and 2°C Global Warming Scenarios." *Nature Climate Change* 8 (May): 375–80. https://doi.org/10.1038/s41558-018-0145-6.

O'Neill, R.V., D.L. DeAngelis, J.B. Waide, and T.F.H. Allen. 1986. *A Hierarchical Concept of Ecosystems*. Volume 23. Princeton, NJ: Princeton University Press.

Paaijmans, K.P., A.F. Read, and M.B. Thomas. 2009. "Understanding the Link between Malaria Risk and Climate." *Proceedings of the National Academy of Sciences of the United States of America* 106 (33): 13844–9. https://doi.org/10.1073/pnas.0903423106.

Paul, A.R. and R. Maity. 2023. "Future Projection of Climate Extremes across Contiguous Northeast India and Bangladesh." *Scientific Reports* 13(1): 15616.

Perkins-Kirkpatrick, S.E., and P.B. Gibson. 2017. "Changes in Regional Heatwave Characteristics as a Function of Increasing Global Temperature." *Scientific Reports* 7 (1): 12256.

Perkins-Kirkpatrick, S.E., and S.C. Lewis. 2020. "Increasing Trends in Regional Heatwaves." *Nature Communications* 11 (1): 3357.

Petley, D.N., 2009. "On the Impact of Urban Landslides." *Geological Society of London, Engineering Geology Special Publications* 22 (1): 83–99. https://doi.org/10.1144/EGSP22.6.

Petri, Y., and K. Caldeira. 2015. "Impacts of Global Warming on Residential Heating and Cooling Degree-Days in the United States." *Scientific Reports* 5 (August): 12427. https://doi.org/10.1038/srep12427.

Phelan, P.E., K. Kaloush, M. Miner, J. Golden, B. Phelan, H. Silva, and R.A. Taylor. 2015. "Urban Heat Island: Mechanisms, Implications, and Possible Remedies." *Annual Review of Environment and Resources* 40 (November): 285–307. https://doi.org/10.1146/annurev-environ-102014-021155.

Qiu, W., and X. Yan. 2020. "The Trend of Heatwave Events in the Northern Hemisphere." *Physics and Chemistry of the Earth, Parts A/B/C* 116: 102855.

Ragettli, M.S., A.M. Vicedo-Cabrera, C. Schindler, and M. Röösli. 2017. "Exploring the Association between Heat and Mortality in Switzerland between 1995 and 2013." *Environmental Research* 158 (October): 703–9. https://doi.org/10.1016/j.envres.2017.07.021.

Rao, K.K., A. Al Mandous, M. Al Ebri, N. Al Hameli, M. Rakib, and S. Al Kaabi. 2024. "Future Changes in the Precipitation Regime over the Arabian Peninsula with Special Emphasis on UAE: Insights from NEX-GDDP CMIP6 Model Simulations." *Scientific Reports* 14(1): 151.

Ren, X., Y. Lu, B.C. O'Neill, and M. Weitzel. 2018. "Economic and Biophysical Impacts on Agriculture under 1.5°C and 2°C Warming." *Environmental Research Letters* 13 (11): 115006. https://doi.org/10.1088/1748-9326/aae6a9.

Riahi, K., D.P. Van Vuuren, E. Kriegler, J. Edmonds, B.C. O'Neill, S. Fujimori, N. Bauer, et al. 2017. "The Shared Socioeconomic Pathways and Their Energy, Land Use, and Greenhouse Gas Emissions Implications: An Overview." *Global Environmental Change* 42 (January): 153–68. https://doi.org/10.1016/j.gloenvcha.2016.05.009.

Riahi, K., R. Schaeffer, J. Arango, K. Calvin, C. Guivarch, T. Hasegawa, K. Jiang, et al. 2022. "Mitigation Pathways Compatible with Long-Term Goals." In *Climate Change 2022: Mitigation of Climate Change*. Contribution of Working Group III to the Sixth Assessment Report of the Intergovernmental Panel on Climate Change, edited by P. R. Shukla, J. Skea, R. Slade, A. Al Khourdajie, R. van Diemen, D. McCollum, M. Pathak, et al. Cambridge and New York: Cambridge University Press. https://doi.org/10.1017/9781009157926.005.

Rosenberg, E.A., P.W. Keys, D.B. Booth, D. Hartley, J. Burkey, A.C. Steinemann, and D.P. Lettenmaier. 2010. "Precipitation Extremes and the Impacts of Climate Change on Stormwater Infrastructure in Washington State." *Climatic Change* 102 (September): 319–49. https://doi.org/10.1007/s10584-010-9847-0.

Ryan, S.J., C.A. Lippi, and F. Zermoglio. 2020. "Shifting Transmission Risk for Malaria in Africa with Climate Change: A Framework for Planning and Intervention." *Malaria Journal* 19 (May): 170. https://doi.org/10.1186/s12936-020-03224-6.

Ryan, S.J., A. McNally, L.R. Johnson, E.A. Mordecai, T. Ben-Horin, K. Paaijmans, and K.D. Lafferty. 2015. "Mapping Physiological Suitability Limits for Malaria in Africa under Climate Change." *Vector-Borne and Zoonotic Diseases*, 15 (12): 718–25.

Sanderson, B.M., Y. Xu, C. Tebaldi, M. Wehner, B. O'Neill, A. Jahn, A.G. Pendergrass, et al. 2017. "Community Climate Simulations to Assess Avoided Impacts in 1.5 and 2°C Futures." *Earth System Dynamics* 8 (3): 827–47. https://doi.org/10.5194/esd-8-827-2017.

Schiavina, M., S. Freire, A. Carioli, and K. MacManus. 2023. "GHS-POP R2023A: GHS Population Grid Multitemporal (1975–2030)." European Commission, Joint Research Centre. https://doi.org/10.2905/2FF68A52-5B5B-4A22-8F40-C41DA8332CFE.

Schleussner, C.-F., T. K. Lissner, E. M. Fischer, J. Wohland, M. Perrette, A. Golly, J. Rogelj, et al. 2016. "Differential Climate Impacts for Policy-Relevant Limits to Global Warming: The Case of 1.5°C and 2°C." *Earth System Dynamics* 7: 327–51. https://doi.org/10.5194/esd-7-327-2016.

Schuster, R.L., and L.M. Highland. 2007. "The Third Hans Cloos Lecture. Urban Landslides: Socioeconomic Impacts and Overview of Mitigative Strategies." *Bulletin of Engineering Geology and the Environment* 66: 1–27. https://doi.org/10.1007/s10064-006-0080-z.

Scoccimarro, E., O. Cattaneo, S. Gualdi, F. Mattion, A. Bizeul, A.M. Risquez, and R. Quadrelli. 2023. "Country-Level Energy Demand for Cooling Has Increased over the Past Two Decades." *Communications Earth & Environment* 4 (1): 208. https://doi.org/10.1038/s43247-023-00878-3.

Sheffield, J., G. Goteti, and E.F. Wood. 2006. Development of a 50-Year High-Resolution Global Dataset of Meteorological Forcings for Land Surface Modeling. *Journal of Climate* 19 (13): 3088–3111.

Sherwood, S.C., and M. Huber. 2010. "An Adaptability Limit to Climate Change Due to Heat Stress." *Proceedings of the National Academy of Sciences of the United States of America* 107 (21): 9552–55. https://doi.org/10.1073/pnas.0913352107.

Sieck, K., C. Nam, L.M. Bouwer, D. Rechid, and D. Jacob. 2021. "Weather Extremes over Europe under 1.5 and 2.0°C Global Warming from HAPPI Regional Climate Ensemble Simulations." *Earth System Dynamics* 12 (2): 457–68. https://doi.org/10.5194/esd-12-457-2021.

Stanke, C., M. Kerac, C. Prudhomme, J. Medlock, and V. Murray. 2013. "Health Effects of Drought: A Systematic Review of the Evidence." *PLoS Currents* 5 (June). https://doi.org/10.1371/currents.dis.7a2cee9e980f91ad7697b570bcc4b004.

Stanley, T., and D.B. Kirschbaum. 2017. "A Heuristic Approach to Global Landslide Susceptibility Mapping." *Natural Hazards* 87 (May): 145–64. https://doi.org/10.1007/s11069-017-2757-y.

Stull, R. 2011. "Wet Bulb Temperature from Relative Humidity and Air Temperature." *Journal of Applied Meteorology and Climatology* 50 (11): 2267–69. https://doi.org/10.1175/JAMC-D-11-0143.1.

Sugg, M., J. Runkle, R. Leeper, H. Bagli, A. Golden, L.H. Handwerger, T. Magee, et al. 2020. "A Scoping Review of Drought Impacts on Health and Society in North America." *Climatic Change* 162 (October): 1177–95. https://doi.org/10.1007/s10584-020-02848-6.

Svoboda, M., M. Hayes, and D.A. Wood. 2012. *Standardized Precipitation Index User Guide*. Geneva: World Meteorological Organization. https://library.wmo.int/idurl/4/39629.

Thrasher, B., W. Wang, A. Michaelis, F. Melton, T. Lee, and R. Nemani. 2022. "NASA Global Daily Downscaled Projections, CMIP6." *Scientific Data* 9 (June): 262. https://doi.org/10.1038/s41597-022-01393-4.

Tilmes, S., D.G. MacMartin, J.T.M. Lenaerts, L. van Kampenhout, L. Muntjewerf, L. Xia, C.S. Harrison, et al. 2020. "Reaching 1.5 and 2.0°C Global Surface Temperature Targets Using Stratospheric Aerosol Geoengineering." *Earth System Dynamics* 11 (3): 579–601. https://doi.org/10.5194/esd-11-579-2020.

Underwood, B.S., Z. Guido, P. Gudipudi, and Y. Feinberg. 2017. "Increased Costs to US Pavement Infrastructure from Future Temperature Rise." *Nature Climate Change* 7 (October): 704–7. https://doi.org/10.1038/nclimate3390.

UNFCCC (United Nations Framework Convention on Climate Change). 2016. The Paris Agreement. Bonn, Germany: UNFCCC Secretariat. https://unfccc.int/sites/default/files/resource/paris-agreement_publication.pdf.Ukey, R., and A.C. Rai. 2021. "Impact of Global Warming on Heating and Cooling Degree Days in Major Indian Cities." *Energy and Buildings* 244 (August): 111050. https://doi.org/10.1016/j.enbuild.2021.111050.

Vecellio, D.J., S.T. Wolf, R.M. Cottle, and W.L. Kenney. 2022. "Evaluating the 35°C Wet-Bulb Temperature Adaptability Threshold for Young, Healthy Subjects (PSU HEAT Project)." *Journal of Applied Physiology* 132 (2): 340–45. https://doi.org/10.1152/japplphysiol.00738.2021.

Vicente-Serrano, S.M., D. Peña-Angulo, S. Beguería, F. Domínguez-Castro, M. Tomás-Burguera, I. Noguera, L Gimeno-Sotelo, and A. El Kenawy. 2022. "Global Drought Trends and Future Projections." *Philosophical Transactions of the Royal Society* A 380 (2238): 20210285.

Vonk, M.A. 2023. "SPEI: A Simple Python Package to Calculate and Visualize Drought Indices (v0.3.5)." Zenodo. https://doi.org/10.5281/zenodo.10816741.Wehrli, K., B.P. Guillod, M. Hauser, M. Leclair, and S.I. Seneviratne. 2019. "Identifying Key Driving Processes of Major Recent Heat Waves." *Journal of Geophysical Research: Atmospheres* 124 (22): 11746–65. https://doi.org/10.1029/2019JD030635.

Wang, T., X. Tu, V.P. Singh, X. Chen, and K. Lin. 2021. "Global Data Assessment and Analysis of Drought Characteristics Based on CMIP6." *Journal of Hydrology* 596: 126091.

Wimberly, M.C., J.K. Davis, M.V. Evans, A. Hess, P.M. Newberry, N. Solano-Asamoah, et al. 2020. "Land Cover Affects Microclimate and Temperature Suitability for Arbovirus Transmission in an Urban Landscape." *PLoS Neglected Tropical Diseases* 14 (9): e0008614. https://doi.org/10.1371/journal.pntd.0008614.

Wong, T., and P. Switzer. 2023. "Estimating Future Local Climate Hazard Probabilities." Technical Note. Washington, DC: World Resources Institute. https://doi.org/10.46830/writn.22.00074.

World Bank. n.d. "World Bank Country and Lending Groups." https://datahelpdesk.worldbank.org/knowledgebase/articles/906519-world-bank-country-and-lending-groups. Accessed November 1, 2023.

Xu, L., N. Chen, and X. Zhang. 2019. "Global Drought Trends under 1.5° and 2°C Warming." *International Journal of Climatology* 39 (4): 2375–85.

Xu, Z., G. FitzGerald, Y. Guo, B. Jalaludin, and S. Tong. 2016. "Impact of Heatwave on Mortality under Different Heatwave Definitions: A Systematic Review and Meta-analysis." *Environment International* 89–90 (April–May): 193–203. https://doi.org/10.1016/j.envint.2016.02.007.

Zhang, F., L.X. Wei, and Y.H. Li. 2023. "Evaluation and Projection of Extreme High Temperature Indices in Southwestern China using NEX-GDDP-CMIP6." *Journal of Meteorological Research* 37(0): 1-20.

Zhang, S., Q. Guo, R. Smyth, and Y. Yao. 2022. "Extreme Temperatures and Residential Electricity Consumption: Evidence from Chinese households." *Energy Economics* 107 (March): 105890. https://doi.org/10.1016/j.eneco.2022.105890.

Zhang, X., N. Chen, H. Sheng, C. Ip, L. Yang, Y. Chen, Z. Sang, et al. 2019. "Urban Drought Challenge to 2030 Sustainable Development Goals." *Science of the Total Environment* 693 (November): 133536. https://doi.org/10.1016/j.scitotenv.2019.07.342.

Zhao, L., K. Oleson, E. Bou-Zeid, E.S. Krayenhoff, A. Bray, Q. Zhu, Z. Zheng, C. Chen, and M. Oppenheimer. 2021. Global Multi-model Projections of Local Urban Climates. *Nature Climate Change*, 11 (2): 152–57.

Zhao, M., J.K.W. Lee, T. Kjellstrom, and W. Cai. 2021. "Assessment of the Economic Impact of Heat-Related Labor Productivity Loss: A Systematic Review." *Climatic Change* 167 (July): 22. https://doi.org/10.1007/s10584-021-03160-7.

ACKNOWLEDGMENTS

This research was supported by Bloomberg Philanthropies.

The authors would like to thank the reviewers and advisers who provided input on this research (unless otherwise noted, organizational affiliations are WRI): Jessy Appavoo (C40 Cities), Alejandro Blei (NYU), Rebecca Carter, Taryn Fransen, Benjamin Jance (Global Covenant of Mayors), Robin King, Marc Manyifika, Paul Switzer (Stanford University), Gregory Taff, Harriet Tregoning, and Elizabeth Wesley.

ABOUT THE AUTHORS

Theodore Wong is a Research and Project Associate on the Data and Tools team at WRI Ross Center for Sustainable Cities.

Contact: ted.wong@wri.org

Eric Mackres is Senior Manager for Data and Tools at WRI Ross Center for Sustainable Cities.

Contact: eric.mackres@wri.org

ABOUT WRI

World Resources Institute is a global research organization that turns big ideas into action at the nexus of environment, economic opportunity, and human well-being.

Our challenge

Natural resources are at the foundation of economic opportunity and human well-being. But today, we are depleting Earth's resources at rates that are not sustainable, endangering economies and people's lives. People depend on clean water, fertile land, healthy forests, and a stable climate. Livable cities and clean energy are essential for a sustainable planet. We must address these urgent, global challenges this decade.

Our vision

We envision an equitable and prosperous planet driven by the wise management of natural resources. We aspire to create a world where the actions of government, business, and communities combine to eliminate poverty and sustain the natural environment for all people.

Our approach

COUNT IT

We start with data. We conduct independent research and draw on the latest technology to develop new insights and recommendations. Our rigorous analysis identifies risks, unveils opportunities, and informs smart strategies. We focus our efforts on influential and emerging economies where the future of sustainability will be determined.

CHANGE IT

We use our research to influence government policies, business strategies, and civil society action. We test projects with communities, companies, and government agencies to build a strong evidence base. Then, we work with partners to deliver change on the ground that alleviates poverty and strengthens society. We hold ourselves accountable to ensure our outcomes will be bold and enduring.

SCALE IT

We don't think small. Once tested, we work with partners to adopt and expand our efforts regionally and globally. We engage with decision-makers to carry out our ideas and elevate our impact. We measure success through government and business actions that improve people's lives and sustain a healthy environment.